NONEQUILIBRIUM MORPHOLOGIES OF RANDOM BLOCK COPOLYMERS PROCESSED BY SOLVENT EVAPORATION

by

Keith Richard Hambrecht

A thesis submitted to the faculty of
The University of Utah
in partial fulfillment of the requirements for the degree of

Master of Science

Department of Materials Science and Engineering

The University of Utah

August 2011

The University of Utah Graduate School

STATEMENT OF THESIS APPROVAL

The thesis of **Keith Richard Hambrecht**

has been approved by the following supervisory committee members:

Grant D. Smith	, Chair	**6/03/11** Date Approved
Dmitry Bedrov	, Member	**6/03/11** Date Approved
Feng Liu	, Member	**6/03/11** Date Approved

and by **Anil V. Virkar**, Chair of the Department of **Materials Science and Engineering**

and by Charles A. Wight, Dean of The Graduate School.

ABSTRACT

This thesis describes the investigation of solvent evaporation processing of random block copolymers and its effects on morphology. Molecular dynamics simulations were performed on a coarse-grained bead spring model of a generic random block copolymer. A standard Lennard-Jones nonbonded potential and a finitely extensible nonlinear elastic (FENE) bonded potential were used. The model was first characterized without the use of solvent processing by 'quenching' the polymer. The Lennard-Jones well depth, ε, was increased for one monomer to produce a block copolymer with blocks of different glass transition temperatures. A co-solvent was then added and the evaporation process was carried out by randomly removing solvent particles from the simulation box. The effect of the solvent evaporation process on morphology was investigated and compared to the quenched polymer. Effect of the strength of solvent, evaporation rate, and Lennard-Jones well depth were all looked at. It was concluded that quenching of random block copolymer melts under conditions where one of the blocks is glassy leads to a kinetically arrested morphology. This morphology has a smaller domain size and more extended chain conformation than the morphology when both blocks are nonglassy. Solvent evaporation processing, however, reduces these effects and produces a larger domain size.

TABLE OF CONTENTS

CHAPTER 1

INTRODUCTION AND BACKGROUND

1.1 Block Copolymers

Block copolymers are very diverse materials that offer varying properties making them candidates for many different applications. Block copolymers consist of two or more polymer chains joined together. Because of this, they can be tailored for specific applications simply by choosing different blocks that have the desired properties. The fact that the different polymers are bonded together prevents macroscopic separation from happening even if it is thermodynamically desired for homopolymer mixtures of these blocks. This creates a wealth of nanoscaled organized structures that depend on the types of polymers and their volume fractions. Long range organization and structure are not realized, but well-defined microphase separation takes place.[1] There are several different structures of block copolymers that can form. Depending upon the application, a certain structure may be preferred over the others. This microphase separation, or self-assembly, is an interesting topic of polymer science and could be extremely useful if it is well understood.

1.2 Block Copolymers as Transport Membranes

Currently, there is a focus in the scientific community on developing new ways to meet our energy demands without contributing to pollution and climate change. Three types of devices have led this push for cleaner energy sources: fuel cells, batteries, and solar cells. Each of these devices offers the ability to produce or store electricity without polluting. There are numerous reasons why each of these devices is not used more widely. One major area of complication that they all have in common is transport membrane issues. The transport membrane, commonly referred to as the electrolyte, serves the purpose of separating the electrodes of these cell devices while selectively transporting charged species from one electrode to the other. The membrane, therefore, must be an electronic insulator. Clearly, the electrolyte plays a major role in operation and must behave properly. If the electrolyte breaks down, the cell will short circuit. If the electrolyte does not transport, or conduct, the respective charged species well enough, the performance with be low. The specific requirements of the electrolyte layer depend on the device. The specific requirements and demands on the electrolyte layer of each device will now be discussed.

1.2.1 Proton Exchange Membrane Fuel Cells

A fuel cell is a device that converts chemical energy into electrical energy. There are several different types of fuel cells, and they are usually named by the type of electrolyte they use. Proton exchange membrane (PEM) fuel cells are fuel cells that transport protons through their electrolyte layer. One of the major applications for PEM fuel cells is for automobile electric motors.

The design requirements for PEM electrolytes include: chemical, mechanical, and electrochemical stability, high proton conductivity, excellent water management, and extremely low permeability to oxygen, carbon dioxide, and hydrogen. The chemical and mechanical stability concerns arise from the need for the membrane to keep the two electrodes separated from each other. The membrane must not degrade from chemicals or gas pressure. Also, the membrane needs to be strong enough to not be damaged during cell assembly. The electrochemical stability concerns arise from the nature of electrochemical devices. It is desired to have these devices operate under a large potential difference, making oxidation or reduction of materials likely. The membrane must have high proton conductivity in order for the fuel cell to produce a significant current. Obviously, this is a major design constraint since the objective of a fuel cell is to produce electricity. Excellent water management means that the membrane must stay hydrated, or be hydrophilic. This is important because water is the proton source so it must be abundant. Low gas permeability is necessary to prevent poisoning of the catalysts in the electrodes and to prevent reactions from taking place inside the cell causing a lack of external electrons to flow. These are the general requirements for the electrolyte layer of PEM fuel cells.

Specifically for automotive applications, it is desired to have these membranes operate at temperatures higher than 120°C and at a low relative humidity of about 20%.[2] There is a large amount of waste heat produced from fuel cells so high temperature stability would reduce the demand of the cooling

system. Operation at low relative humidity would allow from the automobile to be used in low humidity environments without the need of a humidifying system.

Currently, the most common material being used for PEM fuel cells is Nafion™.[3] Nafion™ is a sulfonated tetraflouroethylene random copolymer. As a PEM, however, it offers good performance only below temperatures of 80°C with high humidity. Improved materials are desired but the positive attributes of Nafion™ can provide insight into what materials will be ideal for the application. The molecular structure is the key. What is known about the structure is that a two phase nanoscaled organization promotes proton conduction.[4] The two phases consist of a water-rich domain that carries ions and a semicrystalline phase of the fluorinated blocks that provides mechanical integrity. This combination of an ion conducting phase and a mechanically robust phase is ideal. Therefore, it is desired to engineer a block copolymer membrane for use in PEM fuel cells consisting of a hydrophilic phase for conducting protons and a high strength phase for support that can withstand temperatures of 120°C or higher and sufficiently conduct protons at 20% humidity or less.

1.2.2 Lithium Ion Batteries

Batteries are devices that store electrical energy. A secondary battery is one that can be reused or is rechargeable. One of the most common types of secondary batteries used today is lithium ion batteries. Lithium ion batteries conduct lithium ions through a transport membrane, or electrolyte, from one electrode to the other while electrons flow through an external circuit. The major

application of lithium ion batteries is for small electronic devices such as laptop computers. They are also being considered for automobile electric motors.

The design requirements for lithium ion battery electrolytes are similar to PEM fuel cell electrolytes with some obvious changes. High lithium ion conductivity is desired, rather than proton conductivity. The electrolyte must also dissolve a lithium salt very well in order to have sufficient ions for conduction. An additional consideration is that of the solid/electrolyte interface (SEI). The SEI layer refers to the interface of the electrodes and the electrolyte where reduction or oxidation of the electrolyte occurs over 5-15 nm. The SEI layer causes lower lithium ion conduction through the electrolyte. The electrolyte must form a stable SEI that does not continually lower the ionic conductivity of the membrane.

There are several reasons why a polymer electrolyte would be preferred over the more common liquid electrolytes that are used. A polymer electrolyte is nonvolatile, which would reduce the safety and environmental issues associated with liquid electrolytes. A solid polymer electrolyte would eliminate the need for a separator layer between the electrolyte and electrodes. This would make design of the cell simpler with fewer parts to consider. A third reason to use a polymer is the possibility of using a lithium metal anode, rather than a graphite anode with intercalated lithium. Lithium metal cannot be used as the anode with liquid electrolytes because dendrites of lithium form, which short circuits the cell. With a polymer electrolyte, the additional stiffness may prevent dendrites from forming. The energy density of the cell would be significantly increased if a lithium metal anode was used over a graphite anode.

The main drawback to using a polymer electrolyte is that their lithium ion conductivity is often orders of magnitude lower than liquid electrolytes. This means that elevated temperatures are necessary to get satisfactory conduction.[5] At elevated temperatures of 60°C or more it is likely that most polymer electrolytes, such as polyethylene oxide (PEO), are above their glass transition temperature. Above the glass transition temperature, polymers no longer possess the properties that make them attractive in the first place. They lack the stiffness to be able to eliminate the separator layers and possibly use a lithium metal anode. This leads to the consideration of a block copolymer electrolyte. Optimally, the morphology of block copolymers could provide the combination of mechanical strength and high conductivity. This would allow for higher use temperature or higher conductivity at a lower temperature. Using a block copolymer consisting of a lithium conducting block such as PEO and a stiff block such as polystyrene would make polymer electrolytes feasible for lithium ion batteries.

1.2.3 Organic Solar Cells

A solar cell, also known as a photovoltaic cell, is a device that converts energy from sunlight into electrical energy. There are many different types of solar cells and they use a range of materials. Organic solar cells use organic materials for light absorption, rather than inorganic semiconductor pn junctions. Organic solar cells offer several advantages over other types of solar cells. The main advantage is they are much cheaper and easier to produce than inorganic solar cells that require materials like single crystal silicon. With organic solar

cells, mass producing solar panels at low cost would be possible, and this would make wide spread use of solar energy production much more feasible.

With organic materials, instead of the generation of an unbound electron-hole pair, absorption of light produces a strongly bound electron-hole pair that is referred to as an exciton.[6] In order to utilize excitons in a solar cell they must be separated into an unbound pair. This process of separation takes place at the interface known as the donor-acceptor interface. The donor-acceptor interface is the interface between two materials with mismatched lowest unoccupied molecular orbitals (LUMO). The diffusion length and lifetime of an exciton is about 5-70nm and 1ps – 1ns, respectively. This means that the donor and acceptor layers must be relatively thin otherwise the majority of excitons will decay before they reach the interface and charge separation will not take place. However, if the donor and acceptor layers are very thin then not much light will be absorbed due to lack of ample light absorbing material.

Block copolymers could offer the answer to this issue of membrane thickness optimization. A nanostructured material that features donor-acceptor interfaces throughout would be ideal. A diblock copolymer, consisting of a donor block and an acceptor block, that microphase separates into domains on the order of the exciton diffusion length would be a perfect material. If a membrane made of such a material were used then it could be made thicker without worrying about lack of exciton separation. This would provide ample light absorption for the cell which would increase the overall efficiency of the device.

1.3 Processing of Block Copolymer Membranes

The equilibrium molecular configurations of a block copolymer melt are ones that produce the minimum overall free energy.[7] Since polymer molecules are long and their bulk is viscous true equilibrium morphology typically is never reached due to lack of molecular mobility. This is especially true for block copolymers because the different polymer blocks are bonded together which physically prevents long range segregation. The short range structures that block copolymers ideally form could be very useful, but the ideal structures are not produced in practice. Processing of these polymers must be done in a well understood and controlled manner in order to create structures that are desirable for membrane application.

In order to produce thin films of block copolymers, solvent evaporation processing is utilized.[8] A co-solvent, one that dissolves both polymer blocks, is used to decrease the viscosity of a block polymer. The solution is then either spin-cast or dip-cast onto a substrate. The solvent is then driven off and a thin polymer membrane is left behind on the substrate. The solvent concentration gradient that is developed from the free surface to the substrate creates an ordering front, which propagates down to the substrate. During this process, the rapid solvent evaporation does not allow for thermodynamically preferred, or equilibrium, arrangement to take place but instead can produce interesting bi-continuous or perforated lamellar morphologies. This process provides a route to ordering of nonequilibrium morphologies that can be utilized for membranes. In

order to fully employ this method, however, a better understanding of its effects on the phase separation dynamics of block copolymers is desired so rational process design for membranes can be developed.

This desire for better understanding leads to the necessity for simulations of block copolymers processed by solvent evaporation for membrane applications and others. Computer simulations would allow for viewing of these complex and difficult to predict structures on the molecular scale. This is very important since the structures that form are short range, nanoscaled structures. Experimental study of this scale is difficult, expensive, and potentially uninformative at the molecular scale. The development of simulations tools for studying solvent evaporation processing of block copolymer films is therefore very desirable. Specifically, studying random block copolymers is desired. Random block copolymers are cheaper to synthesize than regular block copolymers. In addition, random block copolymers most commonly produce bicontinuous, nanoscaled structures that are desirable for membranes. This thesis focuses on the development of coarse-grained molecular dynamics (MD) simulations of solvent evaporation processing of random block copolymers.

1.4 Literature Review

This literature review will focus on previous simulation research done that is closely related to the two topics of random block copolymer microphase separation and solvent evaporation processing of block copolymers. There has been very little research done on these specific topics, which is the main motivation for the current research of this thesis; however, there have been a few

related studies that should be mentioned. The related research to be discussed addresses several specific questions including the difficulty of simulating systems of this type, the role solvent parameters play on structure, and what conclusions have been made on the topics of concern.

The need for simulation tools for investigating solvent evaporation processing of block copolymer membranes was discussed in the previous section. What was not discussed is why these simulations are not easy to produce. The difficulty is one reason why progress in this area of simulations has been minimal. The main reason it is so difficult to produce these simulations is the long length and time scales that need to be reached in order to represent the behavior and structure of block copolymers. This is discussed in the paper "Morphology of multi-component polymer systems: single chain in mean field simulation studies" by Daoulas et al.[9] In this paper, the authors explain that the characteristic length scales and relaxation times of soft matter are on the order of nanometers to micrometers and seconds to hours, respectively. This is the reason complicated systems of soft matter must be reduced down to simple models that incorporate the complex details so that computations can access these longer length and time scales without being overly costly. Because polymer molecules are macromolecules, they have correlated conformations along their chain-like backbone that extend for up to a few nanometers. This is a challenge for computations to incorporate such detail over long distances.

One benefit of coarse-grained models is that they can be used to explain the behavior of many different systems. The structures that form with

macromolecules have a degree of universality, which allows similar models to be applied to systems of very different chemical behavior. This commonality in phase behavior is what motivated Daoulas et al to develop models of several different types for application to spinodal decomposition in polymer blends, solvent evaporation from polymer thin films, and self-assembly of diblock copolymers. They compared single chain in mean field simulations with coarse-grained classical molecular dynamics simulations and Monte Carlo simulations. In their simulations they do not discuss, however, specifically random diblock copolymers and the details and implications of their morphology.

The microphase separation behavior of random copolymers was looked at using dissipative particle dynamics (DPD) by Gavrilov et al. in their paper titled "Microphase separation in regular and random copolymer melts by DPD simulations."[10] They were able to establish a relationship between block length of random copolymers and morphology. They found that the mean block length of random block copolymers plays an important role in the structure that forms upon ordering. It was found that with a short mean block length random copolymers formed "rough lamellas" whereas with a longer mean block length bicontinuous structures developed. They compared similar systems of regular and random block copolymers and found some qualitative differences. With regular block copolymers, when the critical χ is reached the transition from order to disorder is abrupt. For random block copolymers, however, this transition takes place over a range of χ values. This paper established simulation data on the structure of

random block copolymers, but it did not investigate the effect that a solvent can have on these structures.

Neratova et al. studied the role of solvent on block copolymer morphology in their paper “Effect of a solvent on self-organization in nanofilms: modeling by the dissipative particle dynamics (DPD) method.”[11] The DPD method is similar to using coarse grained molecular dynamics in that they both use a simple polymer model to achieve longer length and time scales than can be reached in a fully parameterized polymer simulation. In this paper, they were able to show the plasticizing effect of solvent on both a symmetric copolymer processed by solvent evaporation to form defect free lamellar and a nonsymmetric copolymer processed by solvent absorption into the polymer to form a hexagonal structure. In the case of the lamellar solvent evaporation, it was shown that the time to remove defects from the lamellar structure was cut in half compared to a melt system without solvent. This was attributed to the plasticizing effect of the co-solvent and the flow that was created normal to the substrate surface. For the case of the hexagonal structure created by solvent absorption, the ordering of cylindrical domains took place when solvent was absorbed but did not when no solvent was added to the melt. This paper did not investigate random block copolymers nor did it look at behavior of the polymer in the bulk during solvent evaporation, in other words without a free surface.

Tsige and Grest have published several papers on MD simulations of solvent evaporation processing of polymer films.[12] Their first paper, “Molecular dynamics study of the evaporation process in polymer films,” focused on MD

simulations of solvent evaporation of homopolymers on a substrate. They evaporated solvent by removing solvent particles from the top of the box only. This paper looked at the density profiles of the systems as evaporation took place. They were able to provide evidence of an ordering front that propagates through the polymer membrane. This is caused by a density gradient that quickly forms as the solvent at the free surface evaporates much more quickly than in the bulk.

The second paper produced by Tsige and Grest on this topic, “Morphology of evaporated multiblock copolymer membranes studied by molecular dynamics simulations,” took a look at the structures formed by multiblock copolymer thin films produced the same way as the homopolymers in their paper discussed above. They compared AB copolymers where the stiffness of A and B varied and a co-solvent was used. They found that the difference in stiffness between the A and B blocks affected the final morphologies. When there was no difference in stiffness, rough lamellar structures were formed. When the difference in stiffness was small, semilamellar, bicontinuous structures were formed. When the difference in stiffness was large, lamellar structures were not observed, but instead clusters of the stiff chains were surrounded by a matrix of the flexible chains. The structures that were obtained propagated through the membrane and it was determined that the substrate was not necessary for their formation.

The final Tsige and Grest paper is mostly a summary of the first two papers with a closer look at solvent diffusion in to and out of the polymer membranes. Similar conclusions about the morphology were made is this paper.

The Tsige and Grest papers are the most closely related to the research of this thesis and they conclude the literature review of this topic. The aim of this thesis is to make conclusions related to random block copolymer morphology with blocks of different glass transition temperatures since the research described above did not investigate these topics.

1.5 References

1. Hamley, I. *The Physics of Block Copolymers*; Oxford University Press, 1998.

2. Kreuer, K.-D.; Paddison, S. J.; Spohr, E.; Schuster, M. Transport in Proton Conductors for Fuel-Cell Applications: Simulations, Elementary Reactions, and Phenomenology. *Chemical Reviews* **2004,** *104* (10), 4637-4678.

3. Casciola, M. On the decay of Nafion Proton Conductivity at High Temperature and Relative Humidity. *Journal of Power Sources* **2006,** *162* (1), 141.

4. Gierke, T. The Cluster-Network Model of Ion Clustering in Perfluorosulfonated Membranes. *ACS symposium series* **1982,** *180* (Perfluorinated Ionomer Membr.), 283.

5. He, Y. Research Progress on the Polymer Electrolyte. *su liao ke ji* **2009,** *37* (12), 88.

6. Petrova-Koch, V.; Hezel, R.; Goetzberger, A. *High-efficient Low-cost Photovoltaics: Recent Developments*. Springer: 2009.

7. Bates, F. Polymer-Polymer Phase Behavior. *Science* **1991,** *251* (4996), 898.

8. Hamley, I. W. Nanostructure Fabrication Using Block Copolymers. *Nanotechnology* **2003,** *14* (10), R39.

9. Daoulas, K. C.; Muller, M.; de Pablo, J. J.; Nealey, P. F.; Smith, G. D. Morphology of Multi-Component Polymer Systems: Single Chain in Mean Field Simulation Studies. *Soft Matter* **2006,** *2* (7), 573-583.

10. Gavrilov, A. Microphase Separation in Regular and Random Copolymer Melts by DPD Simulations. *Chemical Physics Letters* **2011,** *503* (4-6), 277.

11. Neratova, I. Solvent Effect on Self-Organization in Nanofilms: Modeling Using Dissipative Particle Dynamics. *Vysokomolekulârnye soedineniâ. Seriâ A i seriâ B* **2010,** *52* (9), 1633.

12. (a) Tsige, M.; Grest, G. S. Molecular Dynamics Study of the Evaporation Process in Polymer Films. *Macromolecules* **2004,** *37* (12), 4333-4335; (b) Tsige, M.; Mattsson, T. R.; Grest, G. S. Morphology of Evaporated Multiblock Copolymer Membranes Studied by Molecular Dynamics Simulations. *Macromolecules* **2004,** *37* (24), 9132-9138; (c) Tsige, M.; Grest, G. S. Solvent Evaporation and Interdiffusion in Polymer Films. *Journal of Physics: Condensed Matter* **2005,** *17* (49), S4119.

CHAPTER 2

SIMULATION DETAILS

2.1 The Model

The model chosen for the simulations that were performed had the main criteria that it had to be simple enough to allow long length and time scales, as discussed in the literature review, while still providing the correct qualitative behavior. Therefore, a coarse-grained ideal polymer model was used. The non-bonded potential used was the standard 12-6 Lennard-Jones potential, shown as Equation 2.1. A bead-spring model with a bonded finitely extensible non-linear elastic (FENE) potential, shown as Equation 2.2, was chosen. The values for k and r_0 were 16 and 1.5, respectively.

$$E^{LJ}(r) = 4\varepsilon[(\sigma/r)^{12} - (\sigma/r)^{6} \tag{2.1}$$

$$E^{FENE}(r) = -\tfrac{1}{2}kr_0^2 \ln(1 - (r/r_0)^2) + E^{LJ}(r) \tag{2.2}$$

The reduced units for the systems are defined by ε_{BB} for the energy scale and σ for the distance scale. The cutoff radius for the nonbonded potential was set to 2.5σ. For simplicity, a value of 1 for σ was chosen for all monomers. The reduced temperature, $T^*=k_BT/\varepsilon$, was equal to 1.0. The reduced pressure, $P^*=P\sigma^3/\varepsilon$, was 1.46×10^{-5}. The reduced time step, $t^*= (\varepsilon/m\sigma^2)^{1/2}t$, was 5.467×10^{-3}. In the code used this time step was labeled 1 femtosecond. The time in the results is labeled as nanoseconds, which is 1 million steps of $t^*=5.467\times10^{-3}$, or 1 femtosecond.

2.1.1 Systems Without Solvent - Quenching

The systems consisted of random block copolymers made up of chains of 60 monomers. The total composition was 50% A monomers and 50% B monomers. The chains were composed of 6 blocks of 10 monomers. There were 65 chains of each possible combination of A and B blocks, of which there are 64, represented in Figure 2.1. This created 4160 chains, which produced a system of 249,600 monomers, or particles. This produced a box size of around 65σ x 65σ x 65σ. The compatibility of between the A and B monomers was defined by Equation 2.3. From this equation one can see that if ε_{AA} is greater than 1 and ε_{BB} and ε_{AB} are equal to 1 then χ_{AB} is greater than 0, i.e. A and B will want to phase separate.

$$\chi_{AB} = -\varepsilon_{AB} + \tfrac{1}{2}(\varepsilon_{AA} + \varepsilon_{BB}) \qquad (2.3)$$

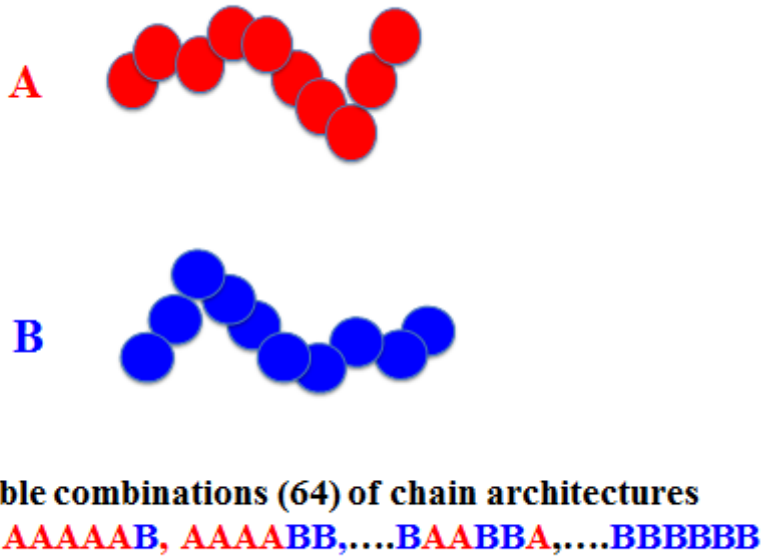

Figure 2.1 - Representation of System

2.1.2 Systems With Solvent

In order to reduce the computational demand, when solvent particles were added to these systems the total number of particles was kept at 249,600. In these systems, there were 1024 chains of 60 monomers, giving 61440 polymer beads and 188160 solvent particles. This made an initial solvent concentration of slightly over 75% for solvent containing systems. The compatibility of the monomers with the solvent particles was defined by Equation 2.4 where M stands for monomer and S stands for solvent.

$$\chi_{MS} = -\varepsilon_{MS} + \tfrac{1}{2}(\varepsilon_{MM} + \varepsilon_{SS}) \quad (2.4)$$

2.2 Equilibrating and Quenching

Before dealing with solvent evaporation, the polymer was studied without solvent in order to develop a baseline to compare solvent evaporation processing with and to gain understanding of the behavior of the model system. To begin, all ε terms were set to a value of 1. This is effectively equivalent to a homopolymer since there is no difference between the A and B monomers at this point. This system was equilibrated in an *NPT* ensemble. Once equilibrated, the ε_{AA} term was changed to values 1.1, 1.3, 1.6, 2.0, and 2.5. The ε_{BB} and ε_{AB} terms were kept at values of 1. Each of these systems was run in an *NPT* ensemble. The process of increasing the ε_{AA} term was termed “quenching” because the temperature of the A blocks was effectively decreased immediately upon changing the ε_{AA} term. Now, these systems are random block copolymers with one block, the A block, having a higher glass transition temperature. The quench systems were examined to establish the baseline behavior of the modeled material. In addition to *NPT* ensembles, the ε_{AA} = 1.6, 2.0, and 2.5 systems were run in an *NVT* ensemble to investigate mechanical properties.

2.3 Addition of Solvent: Equilibration and Evaporation

After studying the quench systems, solvent was added. First, a solvent system was equilibrated with ε_{AA}=1.0 and ε_{AS} and ε_{BS} selected to give a solvent interaction, χ, of -0.5 for both A and B monomers. Hence, a co-solvent was used. In this system alone, a pressure of P*=0.0584 was necessary to prevent the solvent particles from being in the gas phase. Once this system showed a steady radial distribution function, the ε_{AA} term was increased. Five systems were

created. Three systems with values of ε_{AA} of 1.6, 2.0, and 2.5, respectively, were each created with solvent interaction values of -0.5 for both monomers. Additionally, systems of 1.6 and 2.5 were created with solvent interaction values of 0.0 for both monomers.

All of these solvent systems were run in an *NPT* ensemble under the same conditions as the quench systems. They were run until the RDF became steady before the solvent was evaporated. To evaporate the solvent, a predetermined rate was set to remove one random solvent particle from the system every n time steps. The values of n were set to 5, 20, and 50 for each system so the effect of evaporation rate could be examined.

After the solvent was evaporated, with only polymer particles left behind, the systems were run in an *NPT* ensemble until the box size remained constant. Once this happened, the systems were switched to an *NVT* ensemble. Analysis of these systems was run and compared with that of the quench systems. It should be noted that an additional quench system of the same size as the evaporated systems was run to validate comparison between the quench and solvent evaporated systems, which are about 75% smaller.

CHAPTER 3

RESULTS AND DISCUSSION

3.1 Equilibration and Quenching

3.1.1 System Evolution and Snapshots

As discussed in the simulation details, the first step in this project was to develop an understanding of the behavior of the polymer model being used. Most importantly, the effects of increasing the value of the ε_{AA} parameter needed to be investigated. The various polymer systems will be referred to by their ε_{AA} parameter value for the remainder of this thesis.

The time evolution of the structure in the 1.6 system is shown in Figure 3.1. After 2 nanoseconds (ns) a self-assembled structure is already evident; however, the structure continues to develop until about 20 ns where it finally steadies. The 2.5 system differs from the gradually enhancing structure of the other systems. The time evolution of the structure in the 2.5 system is shown in Figure 3.2. There is no change in the structure after 4 ns.

Figure 3.3 shows snapshots of the 1.0 and 2.0 systems, respectively. The influence of quenching is clearly visible from this figure. The A and B monomers phase separate when the attractive interaction between the A monomers is

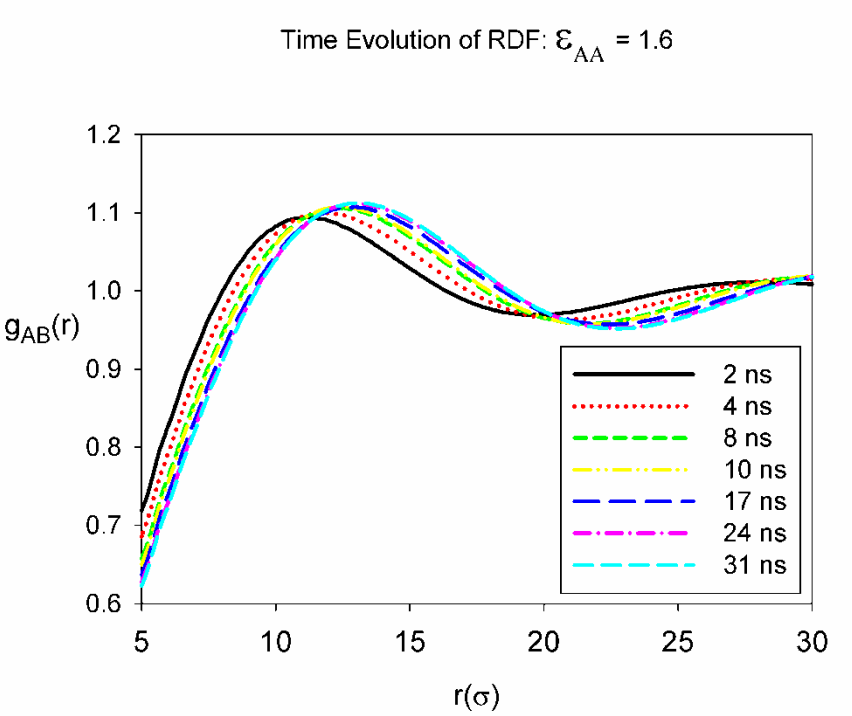

Figure 3.1 – A-B RDF's at various times after increasing ε_{AA} from 1.0 to 1.6.

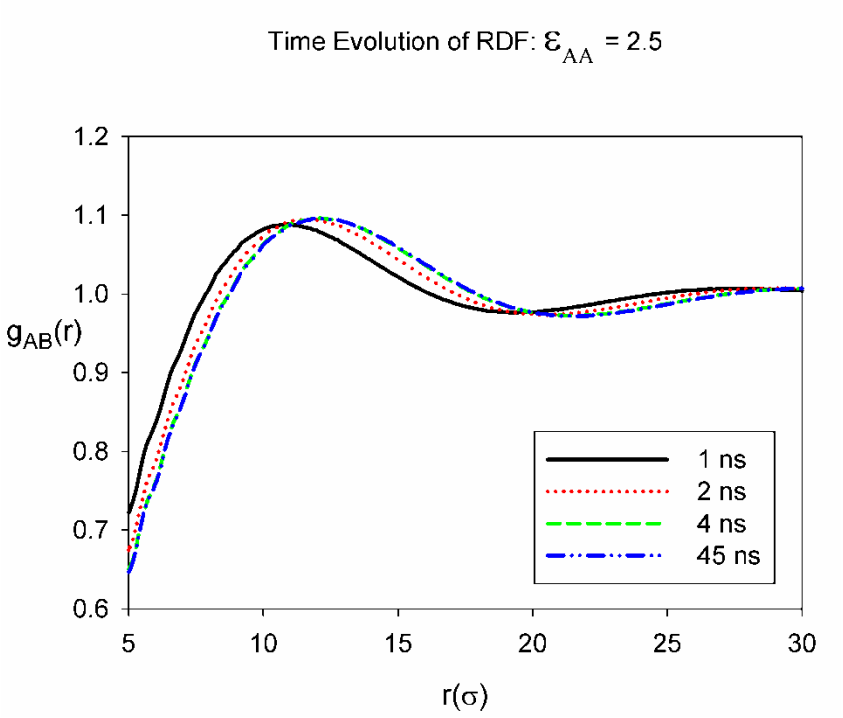

Figure 3.2 – A-B RDF's at various times after increasing ε_{AA} from 1.0 to 2.5.

increased, and a bicontinuous structure is formed. Because the arrangement of the A and B blocks in the chains is random, an orderly and regularly spaced structure is not expected to form.

Figure 3.4 shows a snapshot of the 2.5 quench system in its final configuration. Interestingly enough, the A domains in this system appear to be crystalline. The B monomers are not shown in the figure in order to clearly view the crystallized A domains. The most clearly visible crystallized spots are circled in white; however, when this image is rotated it is evident that all of the A domains are crystalline to some extent. This result was certainly not expected because the block copolymer is random and crystallization of a FENE polymer model has not been previously reported. The influence of the mobile B domains must play an important role in promoting crystallization in this material.

3.1.2 Mean Squared Displacements, Densities, and Radial Distribution Function

The mean squared displacements (MSD) versus time for the A monomers of all the systems are plotted on logarithmic scales in Figure 3.5. It is evident from this plot that as the attraction between the A monomers is increased their motion becomes more restricted. Due to the inverse relationship of ε and the reduced temperature, this is expected. The A monomers have a lower diffusion as their glass transition is raised. All systems show subdiffusive behavior, as expected for polymers. Also, a clear transition in behavior is seen between the 2.0 and 2.5 systems, where a significant drop in displacement happens. The 2.0 A monomers travel around 10σ whereas the 2.5 A monomers do not even travel

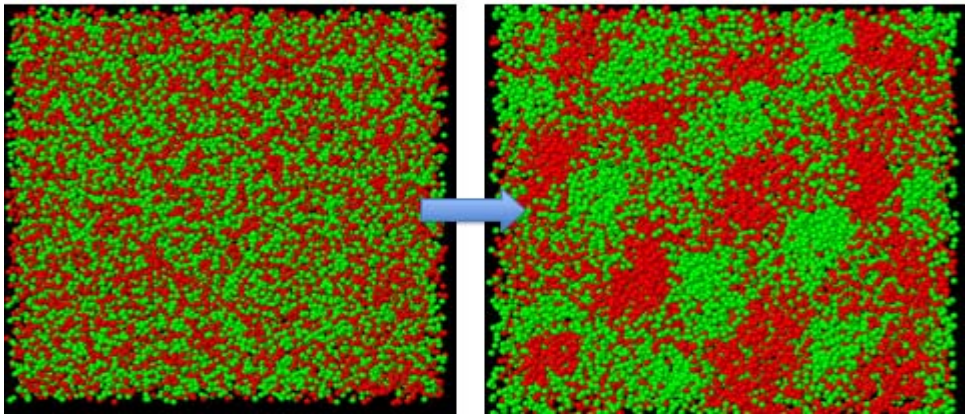

Figure 3.3 – Snapshots of the 1.0 and 2.0 systems, respectively. The A monomers are red and the B monomers are green. The 1.0 shows no organization of A and B monomers since there is no difference between the two in this system. The effect of quenching the A monomers is seen in the 2.0 system with clearly phase separated domains.

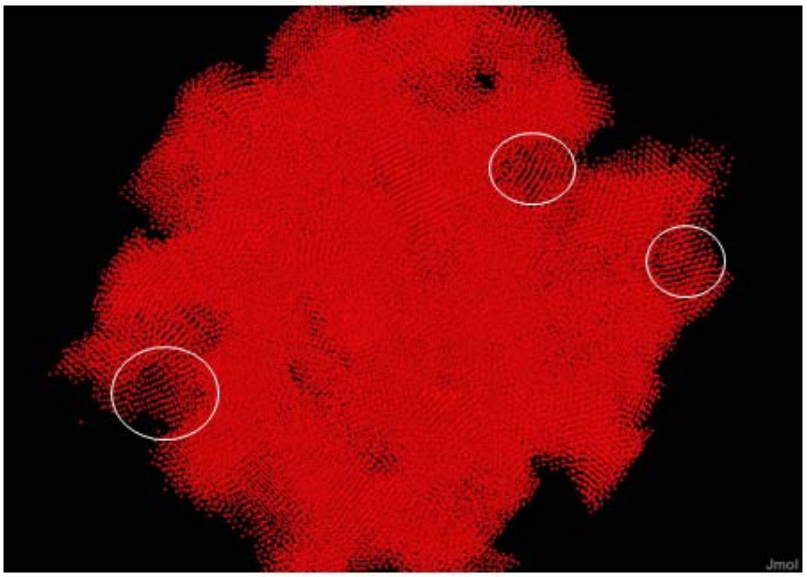

Figure 3.4 – Snapshot of the 2.5 quench system showing the A monomers only in order to view the crystal structure. The white circles point out areas where the crystallization is most easily seen. The B monomer domains do not crystalize.

a distance of 1σ, or 1 bond length. The glass transition temperature for a bulk FENE polymer is about T*=0.41.[1] The A monomers in the 2.5 system have a T* of 0.401, so one would expect to see the large decrease in motion between the 2.0 and 2.5 systems seen in Figure 3.5 because the A monomers are now glassy. For this reason, this plot helped to define the systems of most interest. Investigating the difference in behavior between the systems surrounding the transition regime will be most instructive.

The mean squared displacements versus time for the B monomers of all the systems are plotted on logarithmic scales in Figure 3.6. The first thing to notice is the B monomers have slightly greater MSD's than A monomers. Since the glass transition temperature of the B monomers is lower, this result is expected. The reason the B monomers are not moving much faster, however, is because most of them belong to chains containing A monomers which restrict the motion of the entire chain. Again, a transition between the behavior of the 2.0 and 2.5 systems is evident. In contrast, the B monomers are able to move some before the "caging" effect of the glassy A monomers take effect.

The densities of the quench systems are plotted in Figure 3.7 as a function of ε_{AA}. As expected, the density increases as temperature decreases. One might expect to see an asymptotic limit in the density at the glass transition temperature, but a large increase in the density is observed in this case. The density is significantly increased because the crystallizing of the A domains in the 2.5 system enabled ordered, efficient packing of the monomers.

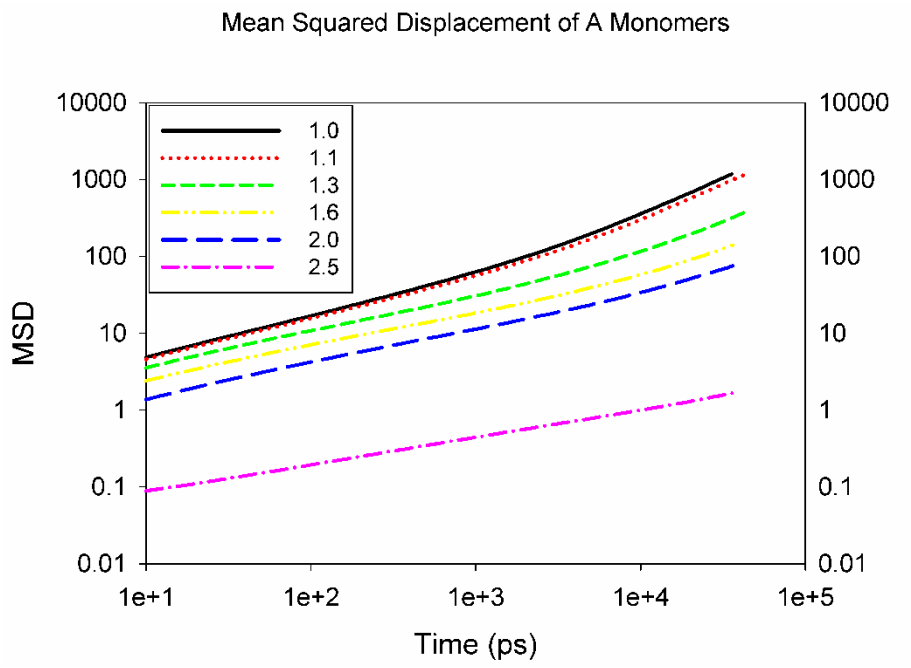

Figure 3.5 - The mean squared displacements of A monomers for all quench systems. The transition between melt and glassy dynamics is observed between the 2.0 and 2.5 systems.

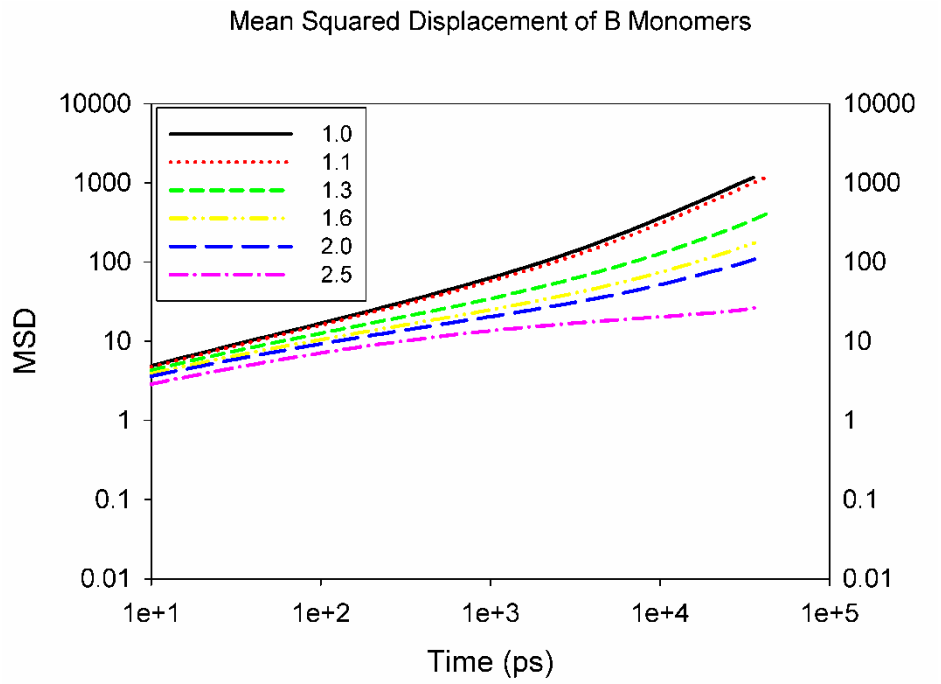

Figure 3.6 – The mean squared displacement of B monomers for all quench systems. The 2.5 system shows asymptotic behavior due to the caging effects of the glassy A blocks.

The A-B RDF's of the final arrested structures of all quench systems are shown in Figure 3.8. The 1.0 system, the black curve, has no longer range structure with the $g_{AB}(r)$ stabilizing to 1 at about 5σ. This shows that the only structure is nearest neighbor arrangement. The 1.1 system, the red curve, shows little variation from the 1.0 system with still no longer range structure, although, there is an increase in the probability of finding an A monomer close to another A monomer. This can be concluded from the $g_{AB}(r)$ having a value less than 1 meaning it is less probable to find a B monomer that distance from an A monomer.

The 1.3 system, the green curve, shows a significant change in structure from the 1.0 and 1.1 systems. With this system, longer range order starts to develop. This is evident from the maximum in the $g_{AB}(r)$ curve at about 11σ. This peak defines the approximate length scale of the self-assembled bicontinuous structure. As ε_{AA} is increased further, to 1.6 and 2.0, this peak is shifted to longer distances with peaks at about 13σ and 15σ, respectively. This indicates that the domains of A monomers are increasing in size.

The 2.5 system, the pink curve, differs from the other trends due to its crystalline nature. Rather than having a maximum in $g_{AB}(r)$ at a slightly greater distance than 2.0, the 2.5 system has a maximum at 12σ, which means it has smaller domains than the 1.6 and 2.0 systems. This can be attributed to the crystalline packing in the 2.5 system. The A domains are more tightly packed leading to smaller domains and a significantly higher density than the 2.0 system.

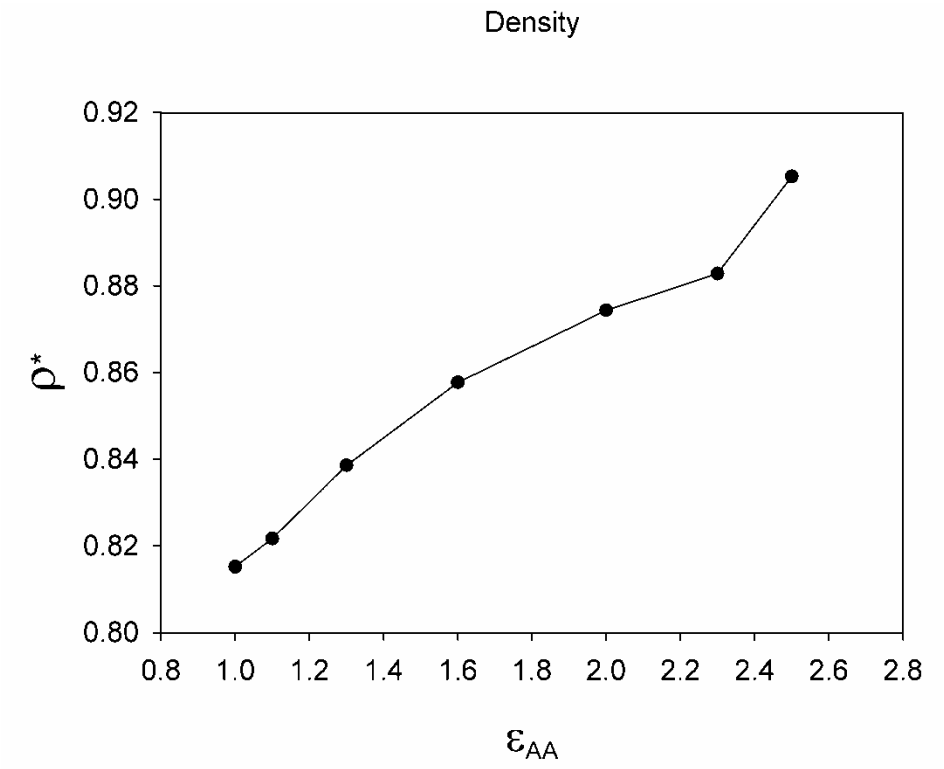

Figure 3.7 – A plot of density versus ε_{AA}. Rather than seeing an asymptotic limit in the density at the glass transition, a large increase in density is observed due to crystal packing effects.

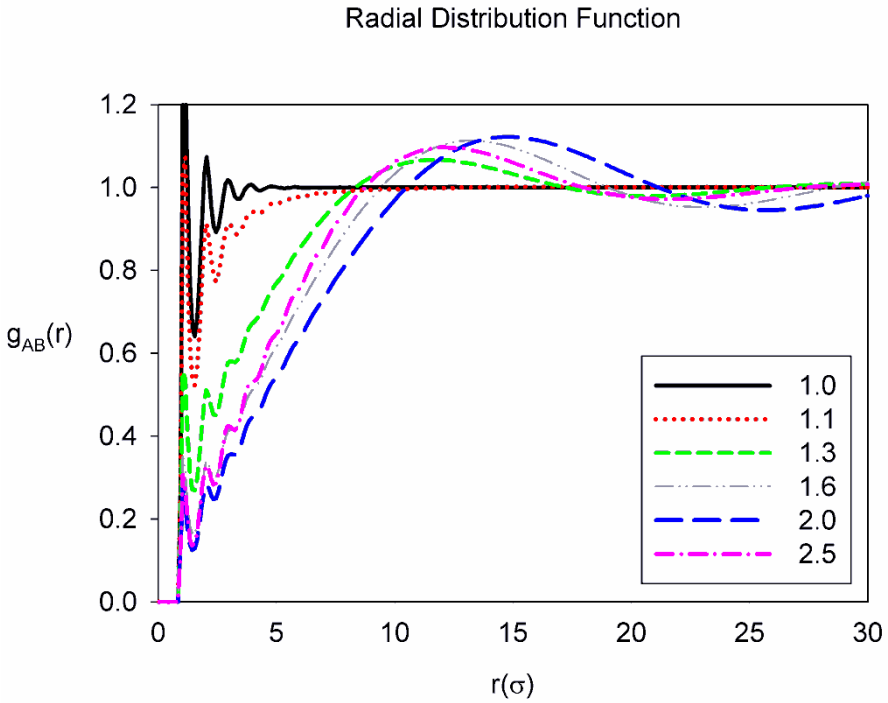

Figure 3.8 – Final A-B radial distribution functions for all quench systems.

3.1.3 Chain Conformations

The radius of gyration of a polymer chain is the mean squared distance to the center of mass of the chain from all points on the chain. It is a convenient measure of the size of polymer chains because it can be measured experimentally as well as from simulations. Figure 3.9 shows the average radius of gyration as a function of the chain composition, or percent of A monomers in the chain, for all quench systems. The chains with all A or all B monomers are the most compact. For all systems other than 2.5, the most extended chains are those containing 50% A monomers. This effect is increased as ε_{AA} is increased.

This distribution of the radius of gyration is expected and can be explained with the compatibility of A and B monomers, χ_{AB}, which is greater than zero meaning A and B want to phase separate. The all A and all B chains are coiled up since the energy is favorable. In an attempt to minimize the energy, the chains containing a mix of A and B monomers are stretched. The monomers are pulled into their respective domains causing a more extended chain structure. As ε_{AA} is increased, the A and B monomers become more incompatible and this stretching and compacting of chains becomes more evident. The 2.5 system curve in Figure 3.9 shows asymmetry, unlike the others, because in this system alone, the A domains are frozen and the B domains are not. The chains containing more B monomers are able to extend further due to their mobility.

The radius of gyration is further investigated in Figure 3.10. The plot shows the radius of gyration as a function of ε_{AA} for 3 different chain compositions. From this plot, one can clearly see that the chains containing half

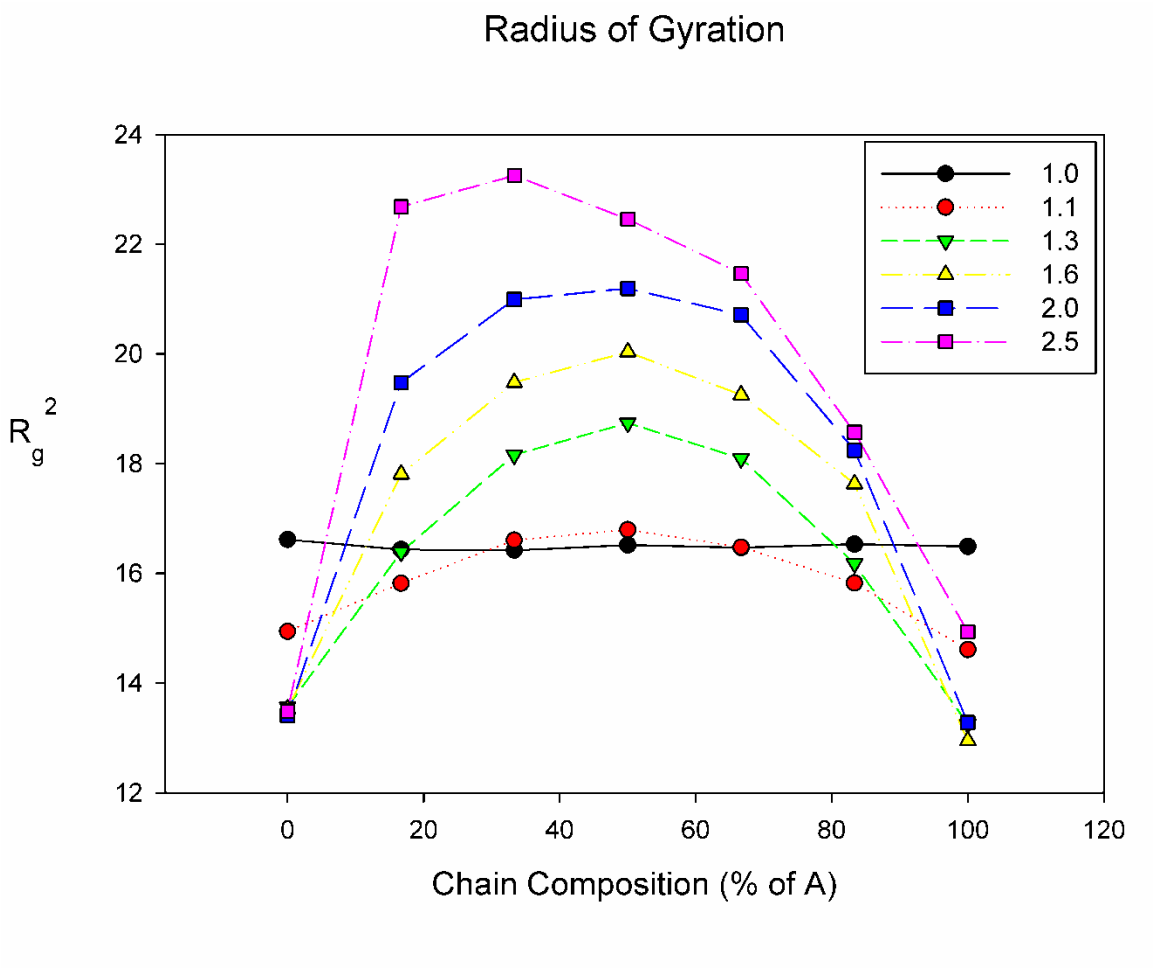

Figure 3.9 – The average radius of gyration versus chain composition for all quench systems. The chains containing all A or all B monomers are the most compact. The asymmetry in the 2.5 system is a result of the crystalline A domains forcing B monomers out of their arranged ordering.

A and half B monomers become more extended as ε_{AA} is increased whereas chains containing all A or all B become more compact. Also, the difference between the behavior of the A and B monomers in the 2.5 system is evident from the fact that the B monomer chains become more compact than the A monomer chains.

Figure 3.11 shows the mean squared end to end distance divided by the radius of gyration plotted as a function of ε_{AA}. A value of 6 for R_e^2/R_g^2 means that the chain is equivalent to a Gaussian chain. From this plot, one can see that the chains containing half A monomers and half B monomers are less coiled than a Gaussian chain. The opposite is true for the all A or all B monomer containing chains.

3.2 Addition of Solvent and Evaporation

From the quenching data results, it was concluded that a high ε_{AA} parameter is necessary to achieve a well phase separated polymer and comparing the difference between well phase separated systems that have glassy A blocks with those that have nonglassy A blocks is the focus of this thesis. That is why solvent evaporation processing of the 1.6, 2.0, and 2.5 systems only were investigated.

The effects on mean squared displacements of adding a cosolvent to the systems will be discussed first. As mentioned in the simulation details a cosolvent with a χ value of -0.5 for both A and B monomers was used for the 1.6, 2.0, and 2.5 systems. In addition, the 1.6 and 2.5 systems were also run with a co-solvent with a χ value of 0. Figure 3.12 shows the A monomer mean squared

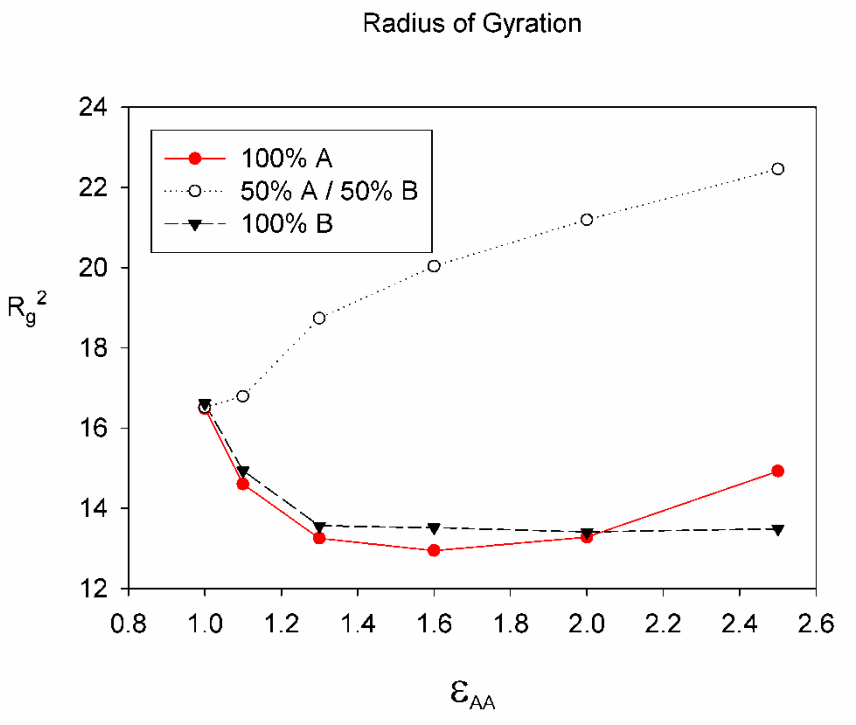

Figure 3.10 – The radius of gyration plotted as a function of ε_{AA} for 3 different chain compositions.

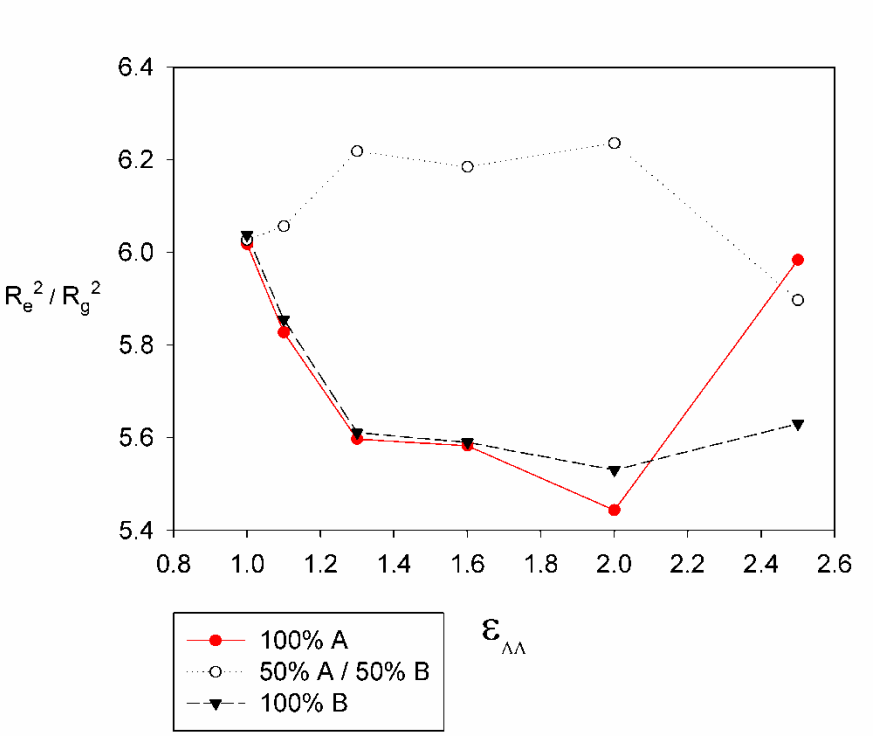

Figure 3.11 – Mean squared end to end distance over radius of gyration plotted as a function of ε_{AA} for 3 different chain compositions.

displacements for all the systems in solution. The systems are still subdiffusive, however, they are moving faster than without solvent. Interestingly, the MSD's for the χ=0 systems are significantly higher. It is possible that with a stronger attraction between the solvent and polymer, the χ= -0.5 systems are inhibited by a larger solvation shell. Figure 3.13 shows the B monomer mean squared displacements and they show the same behavior as the A monomers. Figure 3.14 shows a comparison of the 1.6 system MSD in solution versus without solvent. This plot makes it obvious that the solvent increases the mobility of the monomers. This increased mobility may play a role in increasing the phase separation as the solvent in evaporated.

The impact the solvent had on structure was also investigated. Figure 3.15 shows the $g_{AB}(r)$ for the 2.0 system in solution and without solvent. The peak at 15σ is eliminated when solvent is added meaning that the A and B monomer domains do not exist when the polymer is in solution. This is confirmed in Figure 3.16 which shows snapshots of the 2.0 system quench and 2.0 system in solution, respectively. Clearly, the A and B phase separated domains are not present when the polymer is in solution. The monomers are dispersed by the solvent.

Figure 3.17 shows the time evolution of the radial distribution function of the 2.0 system in solution. This figure was used to determine when it was appropriate to start evaporating solvent from the system. The structure steadied after about 6 to 8 ns. Once the structure was no longer changing, the solvent was evaporated.

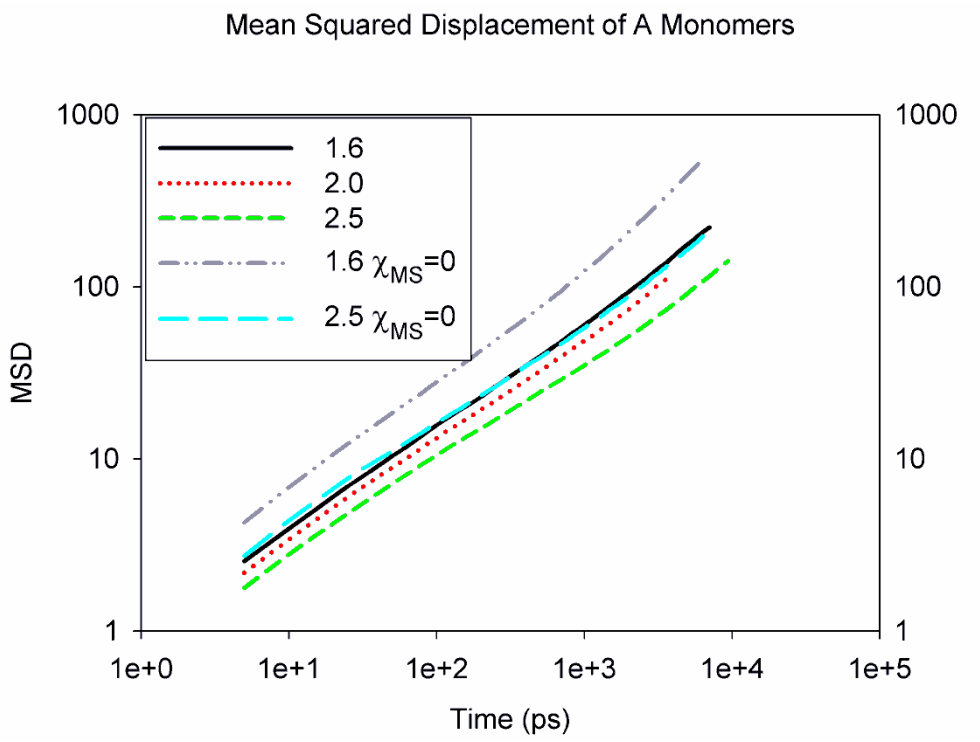

Figure 3.12 – A monomer mean squared displacements versus time of all systems with an added co-solvent.

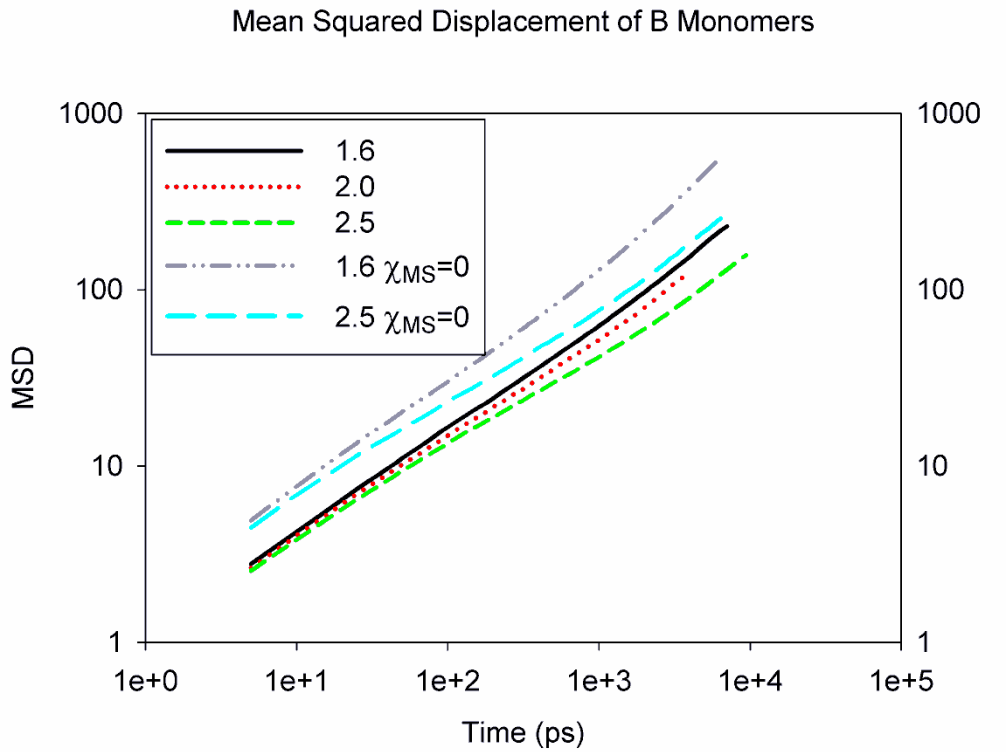

Figure 3.13 - B monomer mean squared displacements versus time of all systems with an added co-solvent.

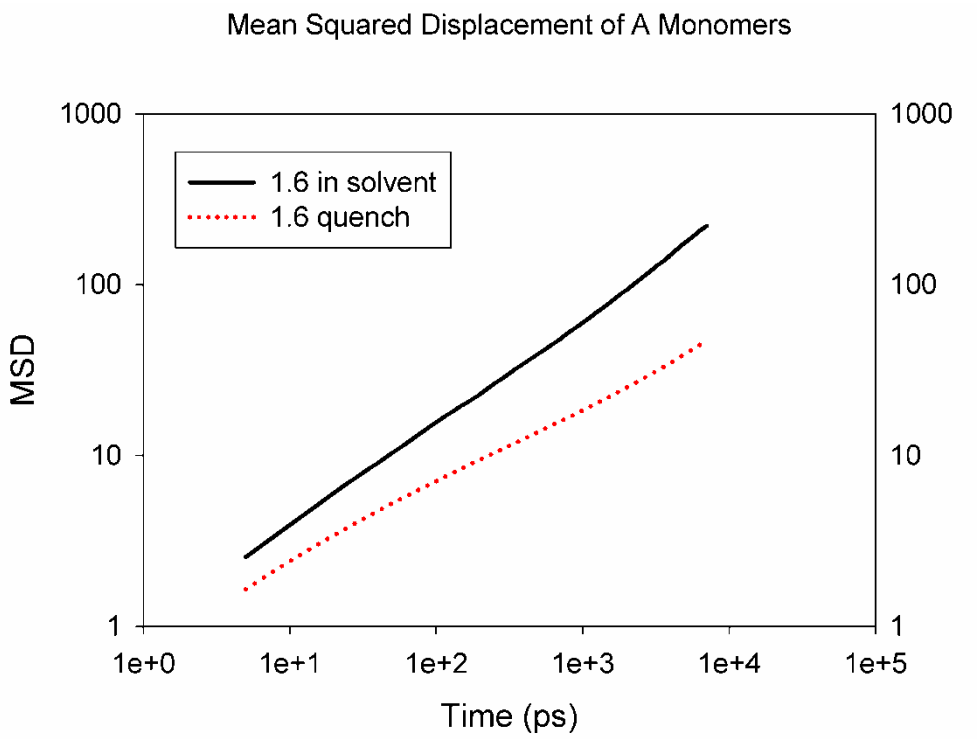

Figure 3.14 – Comparison of the 1.6 system MSD in solution versus without solvent. The solvent clearly increases mobility of the polymer.

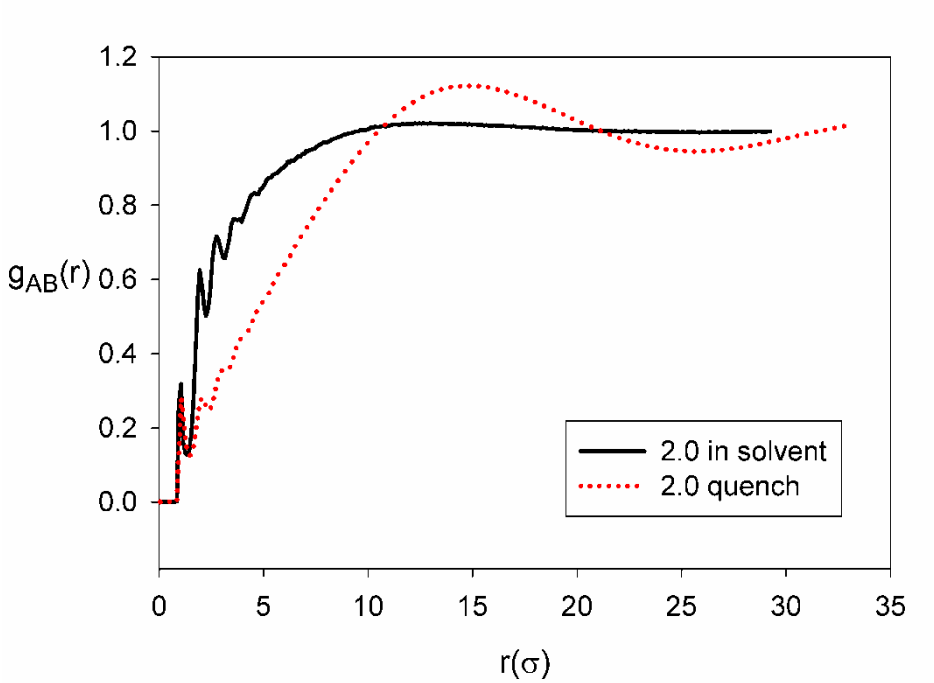

Figure 3.15 – Comparison of the 2.0 system g(r) in solution versus without solvent. The solvent clearly prevents phase separation and large domains from forming.

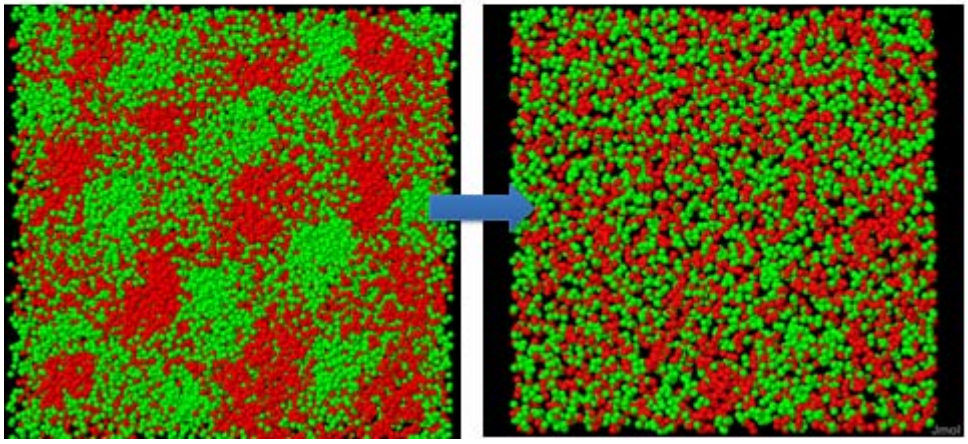

Figure 3.16 – Snapshots of the 2.0 system quench and 2.0 system in solution, respectively. The solvent particles are not shown. Addition of the solvent removes the phase separation in the system.

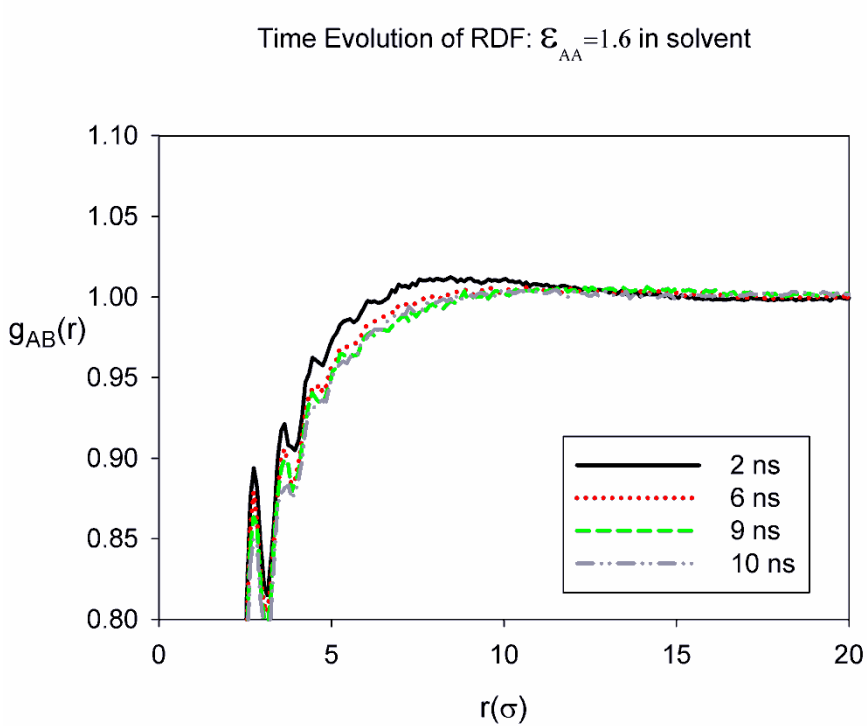

Figure 3.17 – Radial distribution function of the 1.6 system in solution at various times. The system is steady after about 6-8 ns.

The behavior of the solvent as evaporation took place was examined. It was discovered that as phase separation begins to take place, near the end of evaporation, the solvent migrates to the domains of A monomers. This is shown in Figure 3.18, where one can see that the solvent particles are mostly in the A domains. Also, this is evident in Figure 3.19, which shows the AS and BS radial distribution functions. This effect is a result of the definition of χ that was used. In order to have the same χ value for both the A and B monomers, ε_{AS} has to be larger than ε_{BS} creating a larger potential well for the A monomer with the solvent particles. The fact that the system is compressible allows the solvent particles for more efficiently pack into the A domains.

3.3 After Solvent Evaporation

3.3.1 Solvent Evaporation System Comparison

Once solvent evaporation was complete, the structure and behavior of the three systems, 1.6, 2.0, and 2.5, were examined and compared with that of the quench systems. To begin, the $g_{AB}(r)$ was looked at as a function of time after evaporation was complete and compared to the final quench structures. Figure 3.20 shows this for the 1.6 evaporated system with a evaporation rate of 20 (medium rate). The plot focuses on the main peak observed from 8-20σ since this peak defines the characteristic length of the domains. One can see that immediately after evaporation, t=0, the self-assembled A and B domains are less developed than the final, arrested quench structure. Due to the melt nature of this system, however, the structure relaxes over the following 60ns until it reaches the equilibrium structure that the quenched system obtained. The same situation

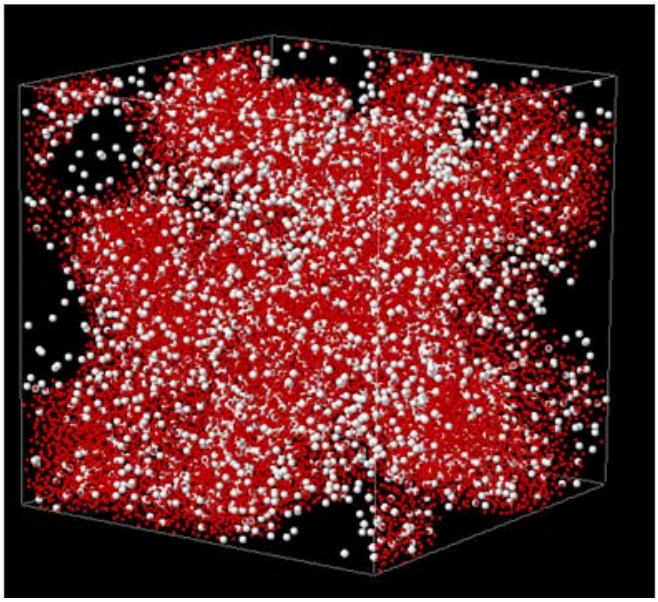

Figure 3.18 – Snapshot of the 1.6 system after 98% of the solvent has evaporated. The A monomers are red and the solvent particles are white. This snapshot exclude the B monomers in order to show that the solvent particles partition to the A domains that begin to form.

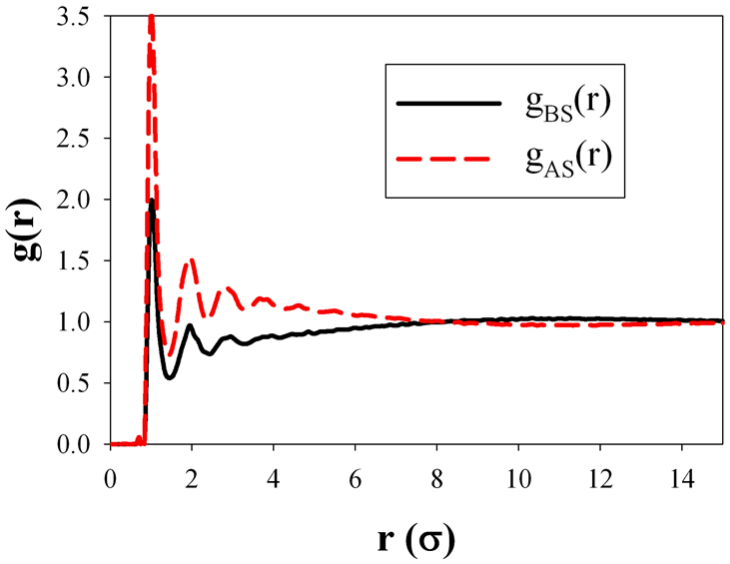

Figure 3.19 – Radial distribution function of 1.6 system after 98% of the solvent has evaporated. It is more likely to find a solvent particle near an A monomer than a B monomer.

was observed for the 2.0 system, shown in Figure 3.21. Since the A blocks of both of these systems are above the glass transition temperature, this relaxation behavior is expected.

In the 2.5 evaporated system much different behavior is observed. From Figure 3.22, one can see that immediately after evaporation, the structure of the 2.5 evaporated system is very similar to the 2.5 final quench structure. The domains appear to extend to a slightly larger size than the quench over the course of 5 ns before becoming arrested. In this system, the combination of the strong driving force for phase separation (large ε_{AA}) and frozen (crystal) nature of the A blocks allowed for a more developed final structure compared to quenching. Also, the same crystallization as the quench system was observed after solvent evaporation processing.

Further comparison to quenching reveals additional differences between the behavior of the 1.6 and 2.0 systems compared to the 2.5 system. Figure 3.23 shows a comparison of the $g_{AB}(r)$ of solvent evaporation versus quenching of the 1.6 system at equivalent times of 1 ns, i.e., 1ns since the process was started. After 1 ns at a evaporation rate of 5, there is no solvent left. It is clear that the quench process creates a more developed structure than the solvent evaporation process over the same amount of time. This is somewhat counter intuitive since the solvent should provide extra mobility for the monomers to move into domains where their energy should be lower. The opposite effect is observed for the 2.5 system, shown in Figure 3.24. In this case, the solvent evaporation process

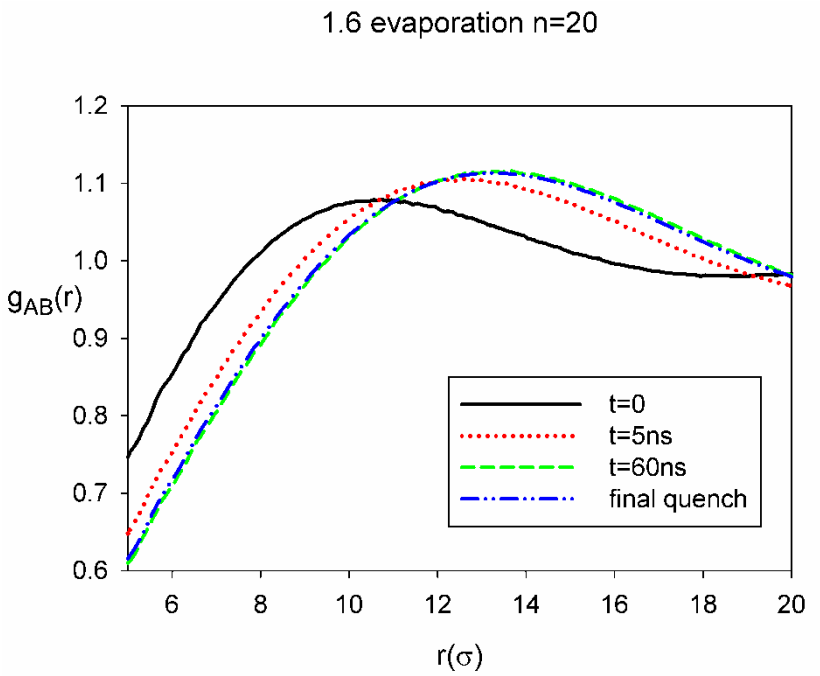

Figure 3.20 – AB radial distribution function for the 1.6 evaporated system at various times after evaporation was complete and compared to the final quench structure.

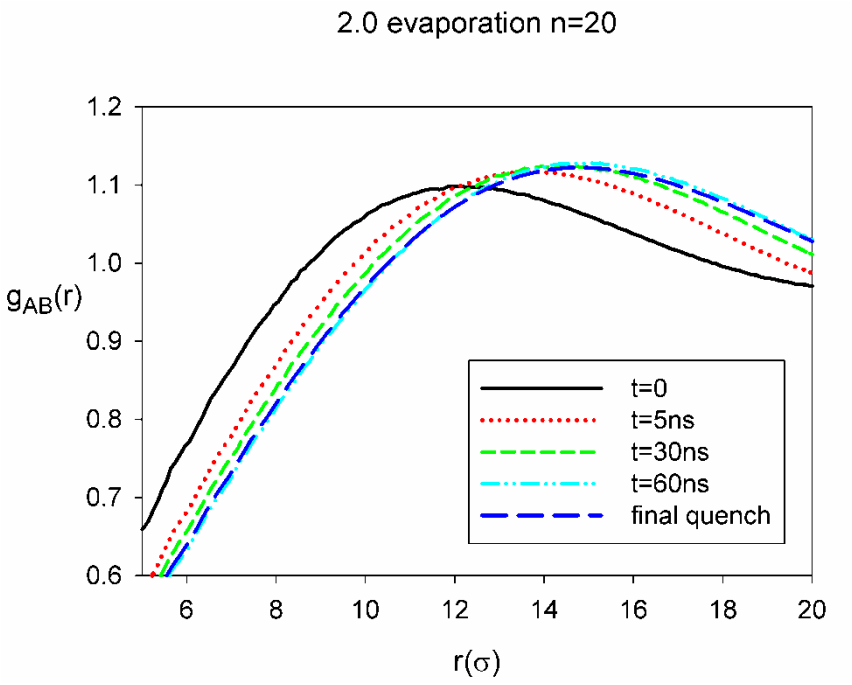

Figure 3.21 - AB radial distribution function for the 2.0 evaporated system at various times after evaporation was complete and compared to the final quench structure.

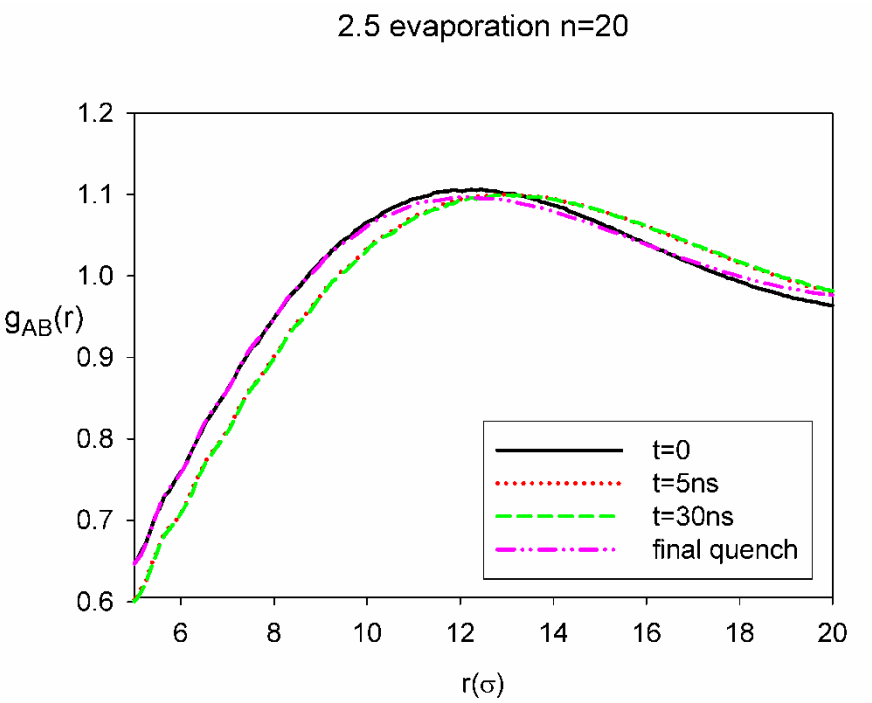

Figure 3.22 - AB radial distribution function for the 2.5 evaporated system at various times after evaporation was complete and compared to the final quench structure.

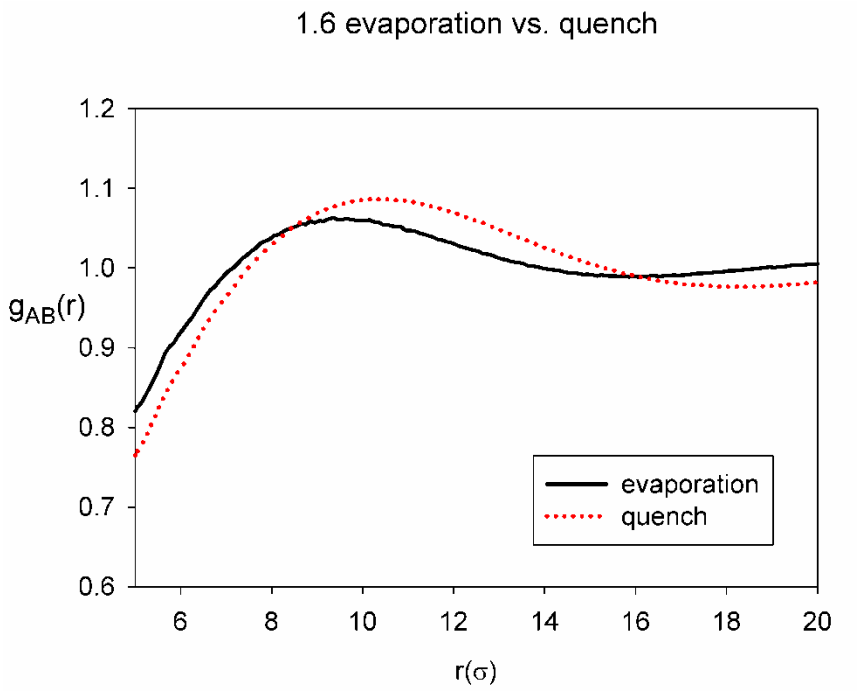

Figure 3.23 – AB radial distribution functions for the 1.6 evaporation system (n=5) and quench system over the same time.

creates a more developed structure than the quench process over the same amount of time.

Comparing Figure 3.25 and Figure 3.26, one can see that immediately after evaporation is complete the 2.5 system has the most enhanced self-assembled structured, but the relaxation of the 1.6 and 2.0 thereafter leaves 2.5 with the least developed structure. Comparing this with the final quench structures in Figure 3.27, however, one can see the end result is that the solvent evaporation processing served the purpose of altering the final structure if one of the blocks is frozen while the other is mobile. Solvent evaporation processing did not have any effect on the final structure of the random block copolymer if both blocks were melt phase. Also, Figure 3.28 shows the density versus ε_{AA} for quenched systems and solvent evaporated systems. The density is not affected by solvent evaporation processing for the 1.6 and 2.0 systems but is decreased in the 2.5 system. Because solvent evaporation processing had no evident final consequence on the 1.6 and 2.0 systems, the effects of solvent evaporation rate and solvent strength will be discussed for the 2.5 system only.

3.3.2 Solvent Strength and Evaporation Rate Effects on Structure

As mentioned in the simulation details, the role of solvent strength and evaporation rate was investigated by using two different solvent strengths and three different evaporation rates. The n=5 rate is the fastest and the n=50 rate is the slowest. The AB RDF's for the three different evaporation rates are plotted for the χ_{MS}=-0.5 and χ_{MS}=0 solvents in Figure 3.29 and Figure 3.30, respectively. For the stronger solvent, χ_{MS}=-0.5, the structure appears to be relatively insensitive to

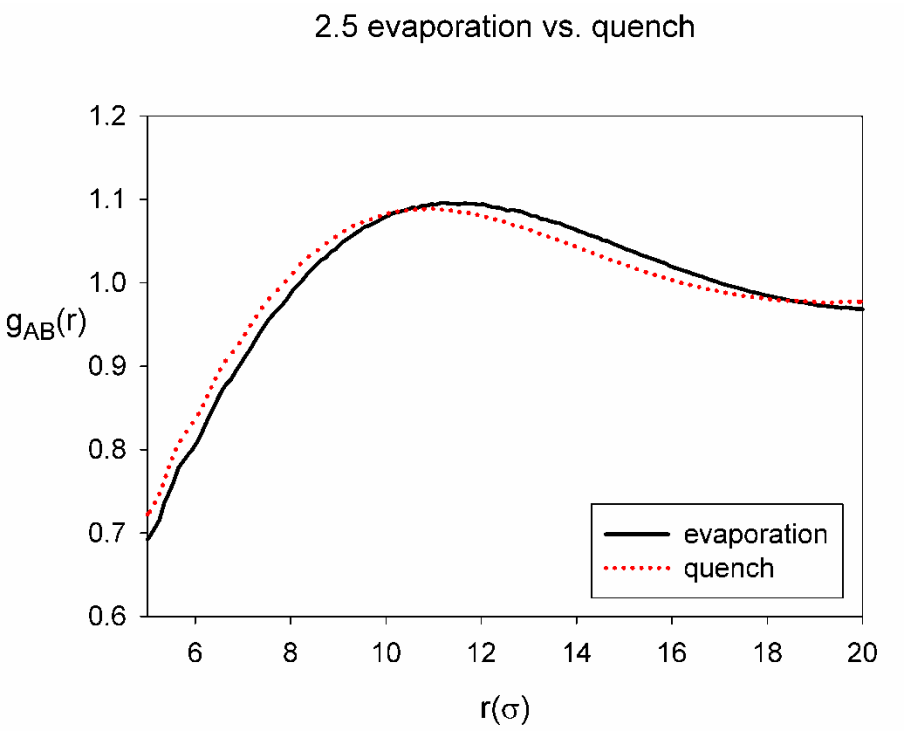

Figure 3.24– AB radial distribution functions for the 2.5 evaporation system (n=5) and quench system over the same time.

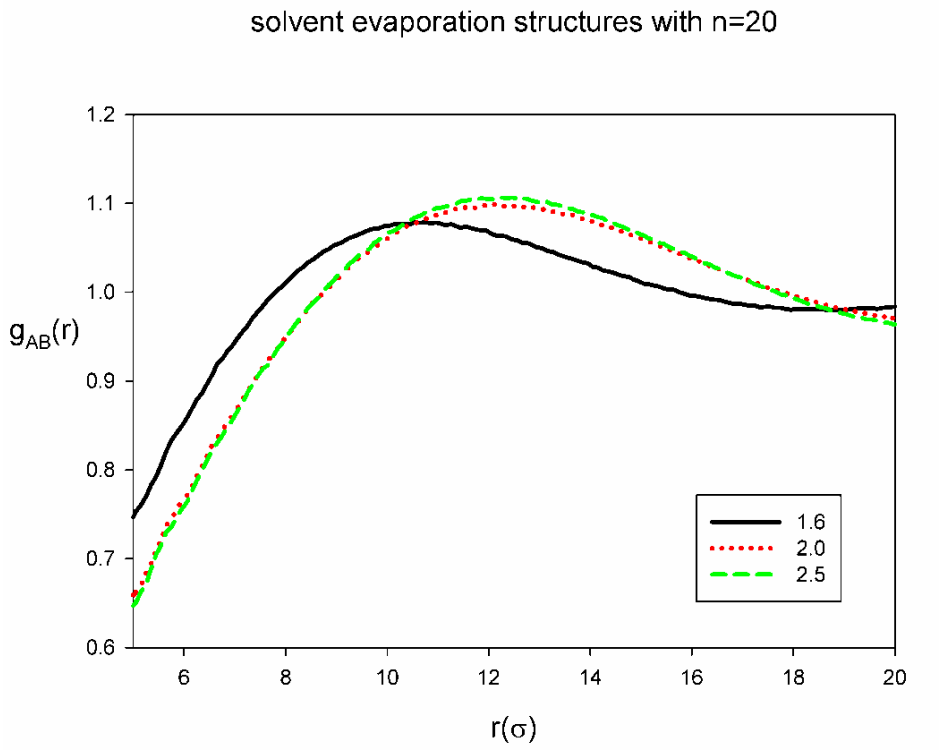

Figure 3.25 – AB radial distribution functions for all systems immediately after all solvent was evaporated.

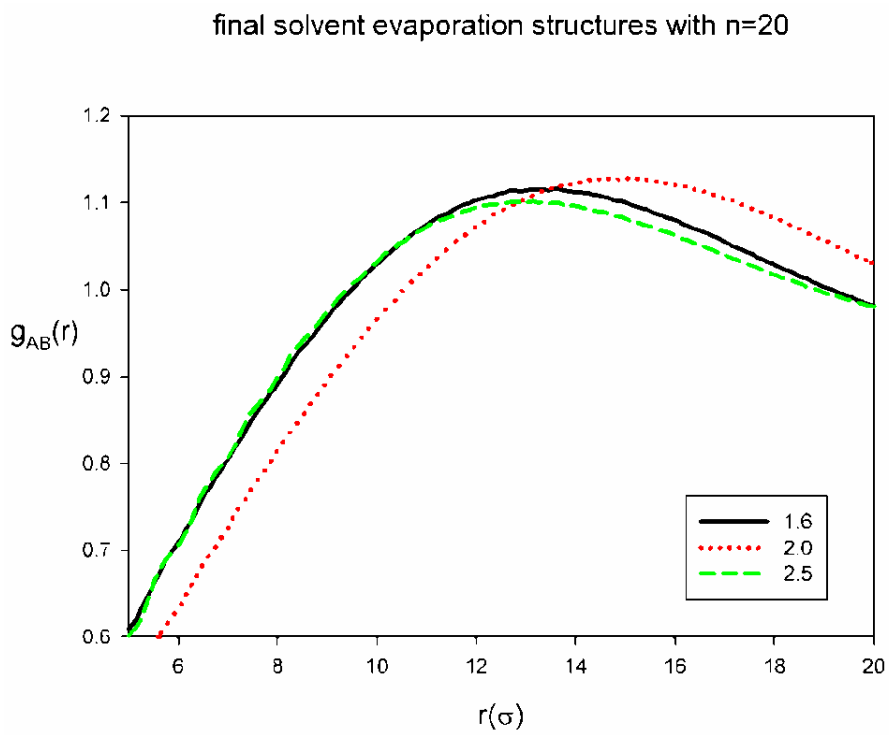

Figure 3.26 – The final AB radial distribution functions for all solvent evaporation systems.

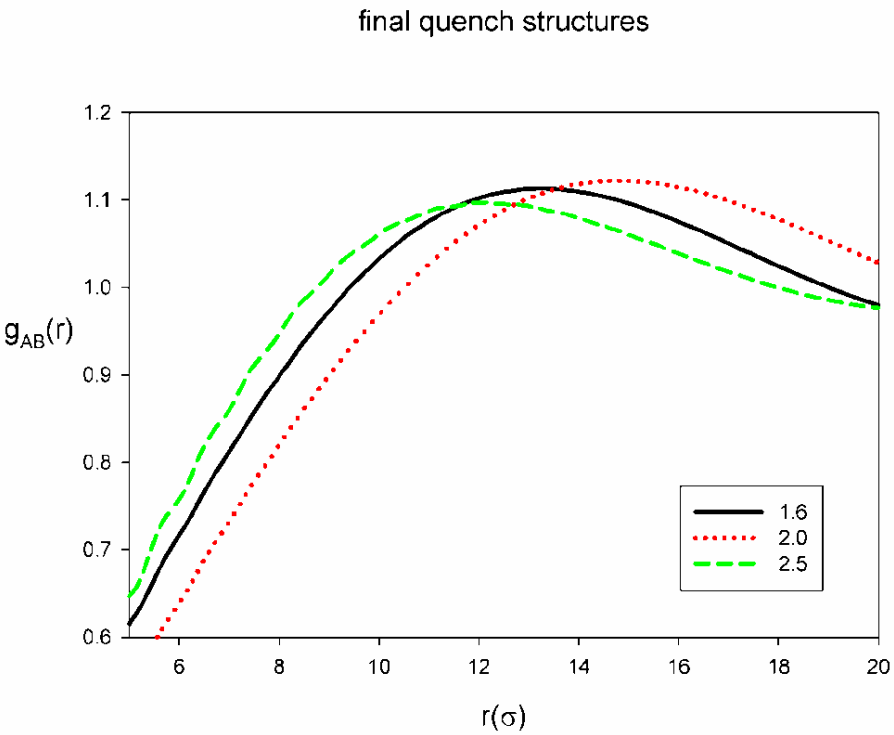

Figure 3.27 – The final AB radial distribution functions for the 1.6, 2.0, and 2.5 quench systems.

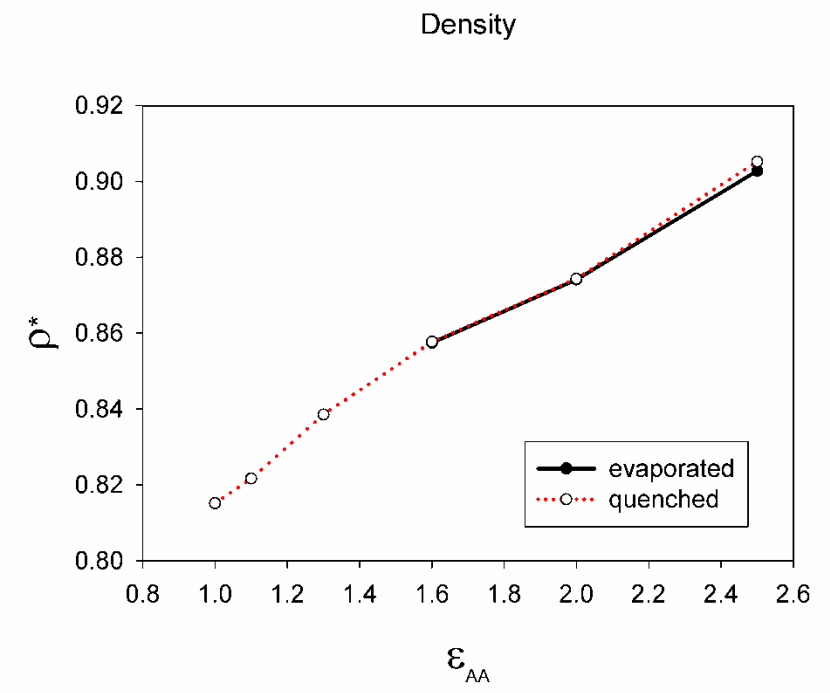

Figure 3.28 – Density as a function of ε_{AA} for quenched systems and χ_{MS}=-0.5 solvent evaporated systems.

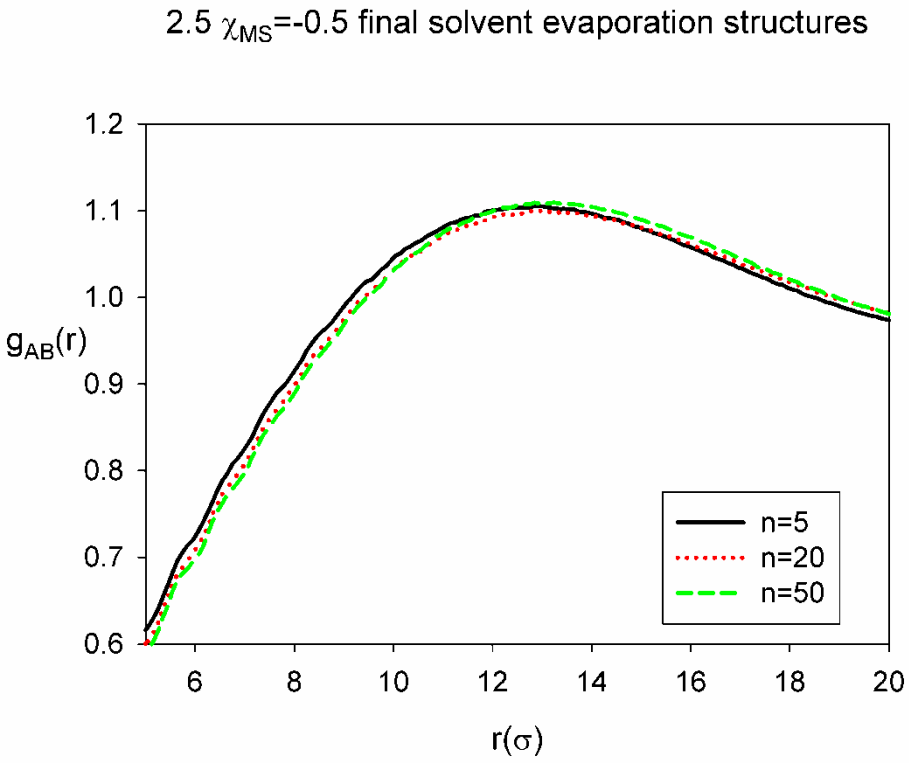

Figure 3.29 – The final AB radial distribution functions for all three evaporation rates for the 2.5 system with χ_{MS}=-0.5.

the evaporation rate. In contrast, the weaker solvent appears to be sensitive to the evaporation rate. When the weaker solvent was used, the slower evaporation rate produced more developed domains of A and B.

When comparing the two solvent strengths at the three different evaporation rates, one can see that the differences in structure are minimal. Figure 3.31, Figure 3.32, and Figure 3.33 are direct comparisons that make this conclusion evident because the peaks in the radial distribution functions are similar for both solvent strengths. However, there are some differences to note. At the slower evaporation rate, the weaker solvent produced larger but slightly less compact domains than the stronger solvent. The stronger solvent was more effective at enhancing the domains when using a fast evaporation rate. The weaker solvent was more effective at enhancing the domains when using a slower evaporation rate.

3.3.3 Solvent Evaporation Effects on Chain Conformations

The radius of gyration versus chain composition for the solvent evaporation systems is compared with the quench systems in Figure 3.34. The 1.6 system's radius of gyration was relatively unaffected by solvent evaporation processing. In Figure 3.34 one can see that the same compositional symmetry is observed for the solvent evaporated 1.6 system as the 1.6 quench system. The same behavior was seen with the 2.0 system (not shown). The radius of gyration in the 2.5 system was significantly influenced by solvent evaporation processing. The radius of gyration was lowered for all compositions except for 100% B chains. This indicates that the chain stretching that was observed in the 2.5

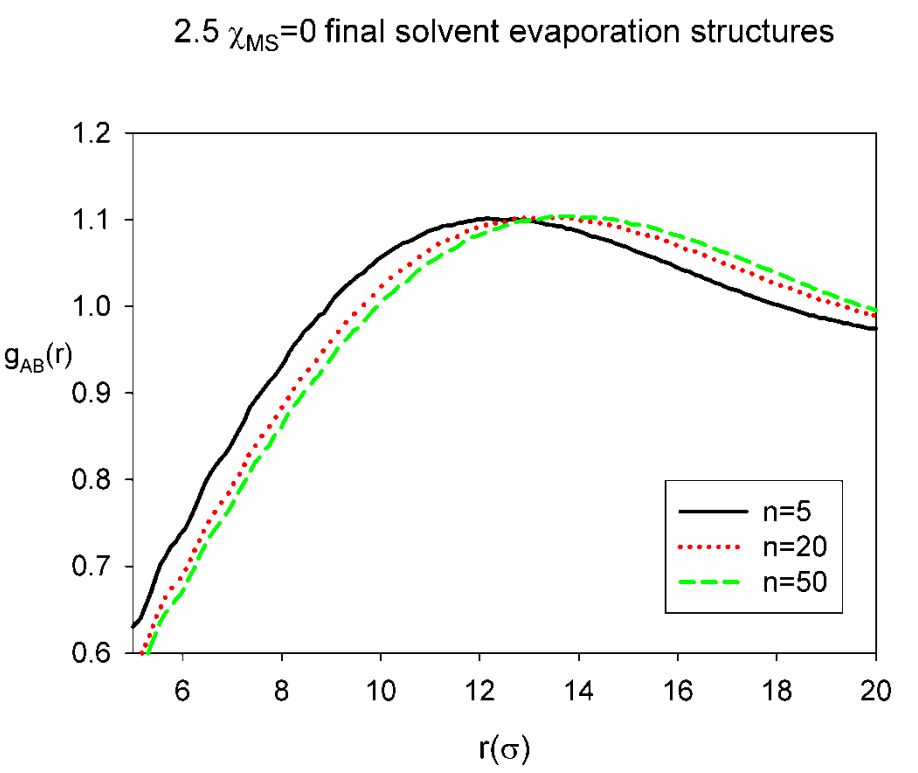

Figure 3.30 - The final AB radial distribution functions for all three evaporation rates for the 2.5 system with χ_{MS}=0.

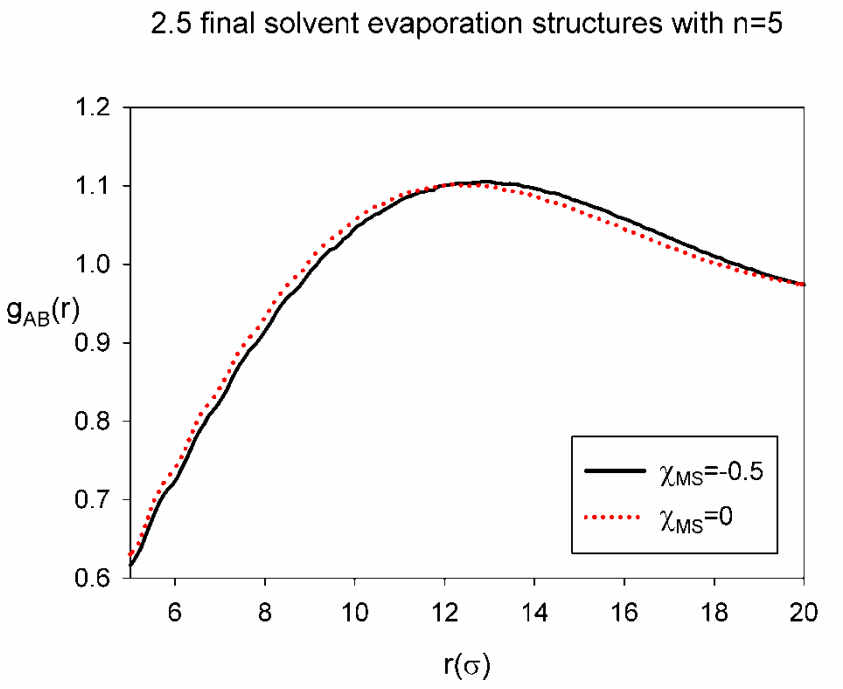

Figure 3.31 – Comparison of the final AB radial distribution functions of the two solvent strengths with the fast evaporation rate.

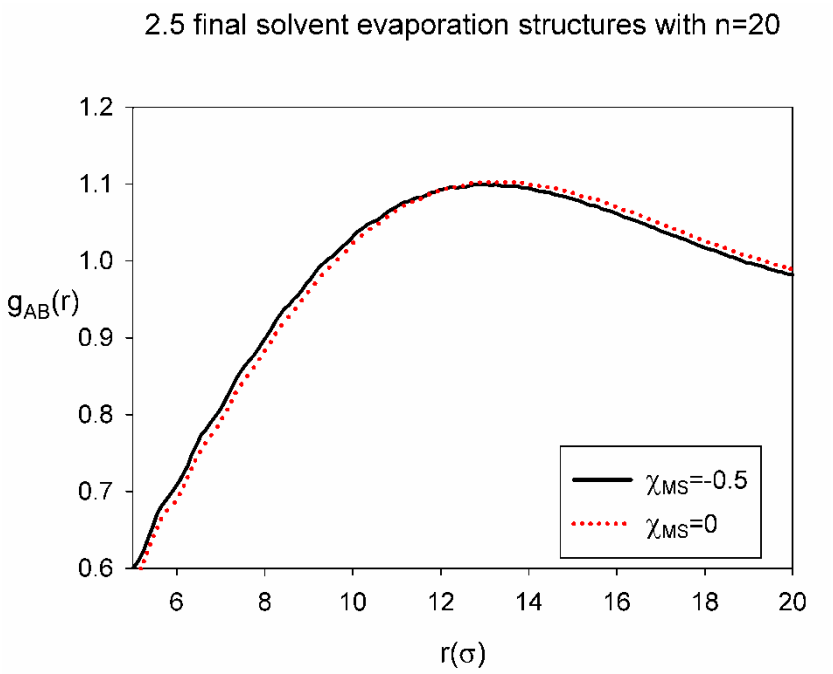

Figure 3.32 - Comparison of the final AB radial distribution functions of the two solvent strengths with the medium evaporation rate.

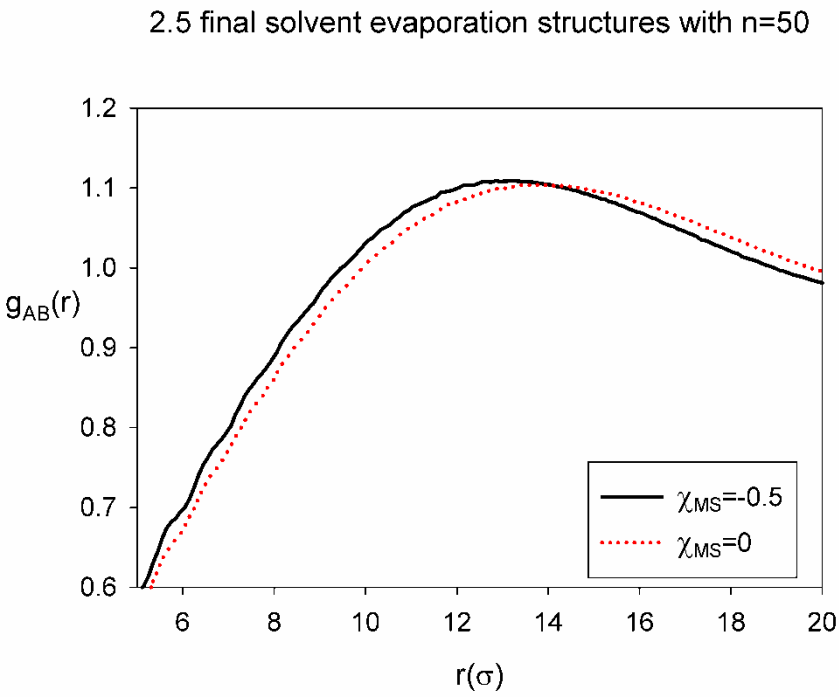

Figure 3.33 - Comparison of the final AB radial distribution functions of the two solvent strengths with the slow evaporation rate.

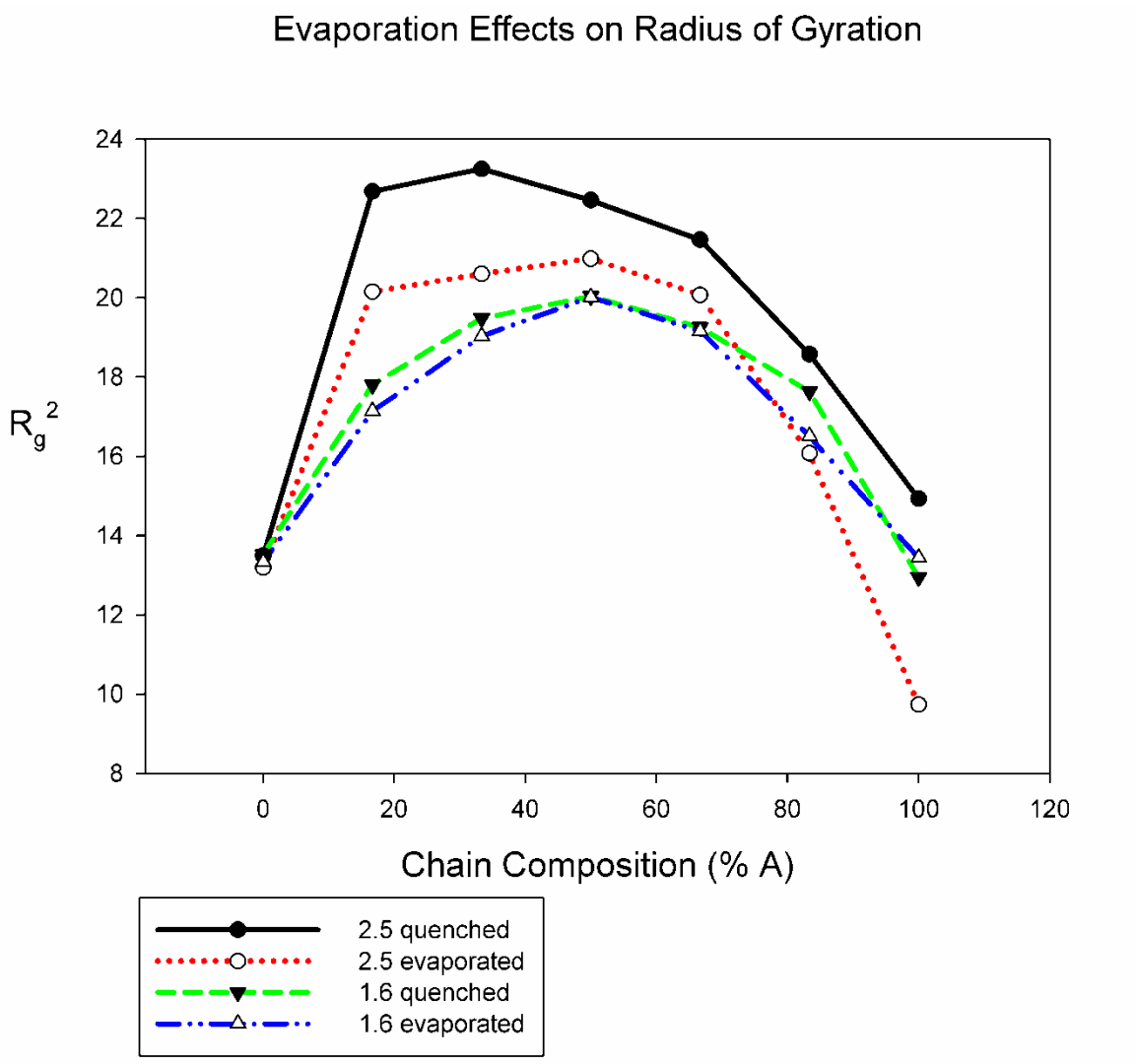

Figure 3.34 – Radius of gyration versus chain composition comparison between solvent evaporation and quenching for the 1.6 and 2.5 systems.

quench system was reduced by solvent evaporation processing. The impact was largest with 100% A chains which appeared to coil up significantly.

The radius of gyration versus ε_{AA} for three chain composition for the solvent evaporated systems is compared with the quench systems in Figure 3.35. The 1.6 and 2.0 systems show no change in radius of gyration, as discussed above. For the 2.5 system, it is clear from this plot that the radius of gyration of 100% B is unaffected. The 50% A chains decreased in radius of gyration by about 3 whereas the 100% A chains decreased in radius of gyration by about 6.

3.4 Conclusions and Future Work

It is desirable to have a random block copolymer that has one glassy block and one non-glassy block for transport membrane applications, however, the glassy block inhibits the development of a preferred structure. Solvent evaporation processing reduces the restrictions from the glassy block. Variables in solvent evaporation processing such as solvent strength and evaporation rate can be used to tune the final structure of the copolymer for a specific membrane application.

It was evident from this work that quenching of random block copolymer melts at conditions where one of the domains is glassy leads to a kinetically arrested morphology with smaller domain size and more extended chain conformations. Solvent evaporation processing reduced these effects. In addition, it was found that solvent strength and evaporation rate play a role in the final outcome of solvent evaporation processing. With a stronger solvent, the

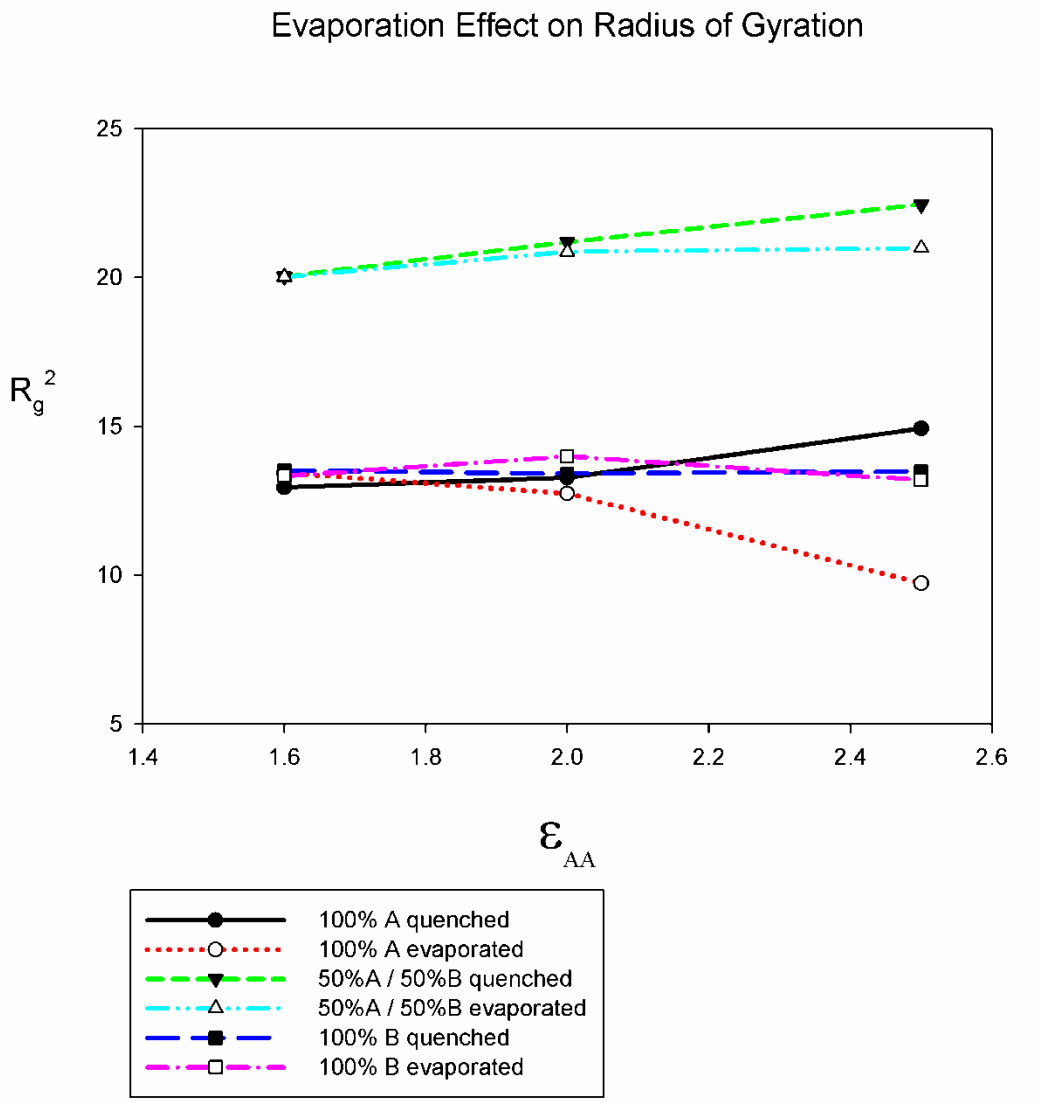

Figure 3.35 – Radius of gyration versus ε_{AA} comparison between solvent evaporation and quenching for three chain compositions.

enhancing of domains was more effective when using a fast evaporation rate than compared to a weaker solvent. With a weaker solvent, the enhancing of domains was more effective with a slower evaporation rate.

Also discovered in this research was the crystallizing of the higher glass transition block, the A block, in both quenching and solvent evaporation processing. This was a very interesting result since the FENE polymer models do not usually produce crystalline polymers, but the interfacial influences of the domains of the phase separated random block copolymer promoted crystallization. This result was not discussed in detail because many more simulations will need to be run in order to fully understand this phenomenon. To investigate this result, simulations will need to be used to figure out what conditions produce crystallization to determine why it is happening. Another system will be run with an ε_{AA} of 2.3 to see if it is possible to have a block of glassy but not crystalline polymer. It will be important to understand what exactly promotes crystallization because the properties of a polymer vary greatly between the crystalline and glass states. In addition to researching the crystallization of the 2.5 system, future work should also include trying to make a connection between this model polymer and real polymers so that solid conclusions can be made that will elicit rational process design of block copolymer transport membranes.

3.5 References

1. Morita, H.; Tanaka, K.; Kajiyama, T.; Nishi, T.; Doi, M., Study of the Glass Transition Temperature of Polymer Surface by Coarse-Grained Molecular Dynamics Simulation. *Macromolecules* **2006,** *39* (18), 6233-6237.